

AERODYNAMICS, KINEMATICS, AND ENERGETICS OF HORIZONTAL FLAPPING FLIGHT IN THE LONG-EARED BAT *PLECOTUS AURITUS*

By ULLA M. NORBERG

Department of Zoology, University of Göteborg, Fack,
S-400 33 Göteborg 33, Sweden

(Received 2 February 1976)

SUMMARY

The kinematics, aerodynamics, and energetics of *Plecotus auritus* in slow horizontal flight, 2.35 m s^{-1} , are analysed. At this speed the inclination of the stroke path is *ca.* 58° to the horizontal, the stroke angle *ca.* 91° , and the stroke frequency *ca.* 11.9 Hz . A method, based on steady-state aerodynamic and momentum theories, is derived to calculate the lift and drag coefficients as averaged over the whole wing and the whole wing-stroke for horizontal flapping flight. This is a further development of Pennycuick's (1968) and Weis-Fogh's (1972) expressions for calculating the lift coefficient. The lift coefficient obtained varies between 1.4 and 1.6, the drag coefficient between 0.4 and 1.2, and the lift:drag ratio between 1.2 and 4.0. The corresponding, calculated, total specific mechanical power output of the wing muscles varies between 27.0 and 40.4 W kg $^{-1}$ body mass. A maximum estimate of mechanical efficiency is 0.26. The aerodynamic efficiency varies between 0.07 and 0.10. The force coefficients, total mechanical power output, and mechanical and aerodynamic efficiencies are all plausible, demonstrating that the slow flapping flight of *Plecotus* is thus explicable by steady-state aerodynamics. The downstroke is the power stroke for the vertical upward forces and the upstroke for the horizontal forward forces.

INTRODUCTION

The long-eared bat, *Plecotus auritus*, is a low-speed flier, is very good in manœuvring, and hovers easily. *Plecotus* has wings of low aspect ratio (Table 2) (i.e. the ratio of the span to the mean chord of the wing). This is calculated as the ratio of the span squared to the wing area:

$$A_r = b^2/A,$$

where b is wing span and A wing area.

The hovering flight of *Plecotus auritus* has been described by Norberg (1970a). Different aspects of bat flight have been investigated in wind-tunnel experiments: Pennycuick (1971) studied the gliding performance of *Rousettus aegyptiacus*, Schnitzler (1971) measured wing-beat frequency as a function of wind speed in *Myotis lucifugus*,

and Thomas & Suthers (1972) and Thomas (1975) measured the oxygen consumption of the horizontal flight of *Phyllostomus hastatus* and of *Pteropus gouldii*.

Weis-Fogh (1972, 1973) has shown that hovering flight in humming-birds and several insects is consistent with steady-state aerodynamics. Some insects make use of non-steady-state aerodynamics (Weis-Fogh, 1972; R. Å. Norberg, 1975), and hovering flight in the pied flycatcher (*Ficedula hypoleuca*) has to be explained by non-steady-state phenomena (U. M. Norberg, 1975).

The purpose of this investigation of *Plecotus auritus* is: (1) to describe the kinematics during horizontal flight; (2) to estimate the forces elicited by the wings during various phases of the stroke cycle; (3) to calculate the force coefficients, C_L and C_D (averaged over a whole wing-beat cycle) and to find out if slow horizontal flight is consistent with steady-state aerodynamics, or has to be explained partly by non-steady-state phenomena; (4) to evaluate the absolute and relative effect of the down- and upstrokes, and (5) to calculate the aerodynamic work and power needed for slow horizontal flight.

Quantitative and qualitative analyses of aerodynamics require data on several quantities. These are not constant during the wing-beat cycle or at different parts of the wing during the wing movements. For example, the directions and velocities of the relative wind, the local angle of attack, the force coefficients, and the resultant force are different in every phase of the cycle and for every strip of the wing. Further, to calculate the vertical component of the resultant force one has to take into consideration that the direction of the resultant force changes both laterally and antero-posteriorly during the wing-beat cycle. In addition, the wings are flexed during most of the upstroke. Because there are so many variables, the sources of errors are many, and hence a detailed investigation of the aerodynamics is very difficult to make.

MATERIAL

Films and measurements were made on the long-eared bat *Plecotus auritus* (Linnaeus) (Microchiroptera, Vespertilionidae). Three different specimens were used for cine films, still pictures, and wing measurements, respectively. The weight used in calculations refers to the specimen filmed. The span of the bat filmed and of the bat used for wing measurements were equal.

METHODS

Filming and photographing

The bats were filmed and photographed in the laboratory, as they flew horizontally in a net cage, $0.6 \times 0.6 \times 3.5$ m. As no solid walls were closer than *ca.* 1 m to the bats, interference with the airstream around the wings may be neglected. The filming section was in the centre of the cage, and measured $0.6 \times 0.6 \times 0.85$ m. A string grid, forming 2×2 cm squares, was used as a background scale when analysing the films, allowance being made for the distance between the grid and the bat.

A mirror, tilted 45° to the horizontal and placed under the filming section, was used for filming the ventral view. Lateral, ventral, front (or back) views were obtained from different flights. Front and back views were sometimes obtained from the same flight, when the bat turned in the net tunnel.

The bats flew spontaneously to and fro without training. The bat was released from the experimenter's hand at one end of the cage from where it took off. It flew for up to four cage lengths before landing. The film camera was triggered before the bat took off, so as to allow acceleration of the film.

About 800 m of film was taken with a Kodak 16 mm high-speed film camera (time-marking each 1/100 s) with rotating movement compensating prism. The speeds used varied between 200 and 1000 frames s⁻¹. The bat was illuminated with 4500 W photo lamps, mounted approximately 1 m to the side of the flight path. Ilford FP 3, Ilford HP 3, and Kodak Tri-X Reversal films were used.

Still pictures of the flying bat were taken simultaneously with three cameras, from the side, in front and from below. The cameras used were a Leicaflex SL (side view), a Leica M 3 (frontal view), and a Pentax SL (ventral view). The photographs were taken with two electronic flashes (exposure time 0.1 ms), mounted above the bat, so that the bat was illuminated obliquely from in front and obliquely from behind. The shutters of the cameras were held open, and the exposures made when one flashgun was triggered manually and, in turn, triggered the second flashgun via a photocell. The film used was Kodak Panatomic X.

Coefficients of lift and drag

If steady-state aerodynamics are adequate to explain horizontal flight, the average lift coefficient must not exceed the maximum coefficient of lift obtainable at the Reynolds number under which the wings operate. Both C_L and C_D are estimated for horizontal flight by a method which is a further development of Pennycuick's (1968) and Weis-Fogh's (1972) expressions for estimating the average lift coefficient in flapping flight. Pennycuick found the average resultant force coefficient, C_F , by setting the vertical components of the resultant force for the whole wing and wing-stroke equal to the weight of the animal (pigeon). He then found the lift coefficient from his program by iteration and the L/D ratio from wind-tunnel measurements of a gliding pigeon. His calculations refers only to the downstroke. Weis-Fogh assumed an L/D ratio and also calculated the lift coefficient by setting the vertical components of the resultant force for the entire wing and wing-stroke equal to the weight of the animal. He did not separate the upstroke from the downstroke, but made calculations for half a downstroke and multiplied the value by 4, since humming-birds and several insects have a rather symmetrical stroke in hovering flight.

My method differs from theirs in the following respects. (1) The vertical components of the *lift* and *drag* forces for the whole wing and wing-stroke are added, to balance the weight of the bat. Similarly, the horizontal components of the *lift* and *drag* forces are added, to balance the body drag of the bat. The lift and drag coefficients, and thus the lift:drag ratio, can be directly solved from these relations. (2) The upstroke is treated separately in this investigation, because it is so different from the downstroke. This method is described in detail below (p. 188).

Power requirements

The aerodynamic work and power required for horizontal flight is calculated by the use of Weis-Fogh's formulae (1972), with some modifications applicable for horizontal flight. These are given below (p. 203).

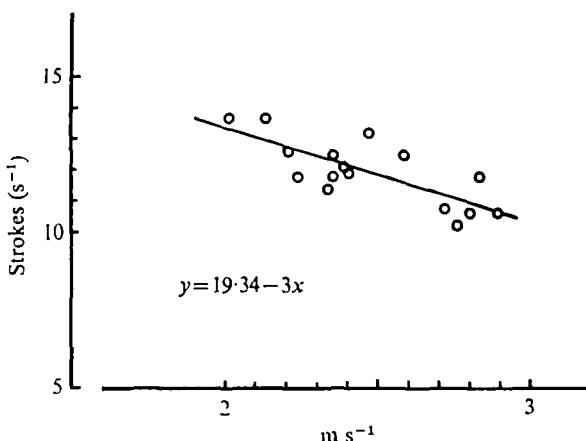


Fig. 1. Wing-stroke frequency plotted against the flight speed for the bat. The regression equation is only valid for the speed range 2–3 m s⁻¹, for which data is available.

DEFINITIONS

The *wing length*, R , is the distance between the humeroscapular joint and the wing tip.

The *wing span*, b , is the distance between the two wing tips when the wing is fully extended as during the downstroke.

The *wing area*, A , is the area of both wings (as projected on the wing chord plane) and the portion of body in between.

The *arm wing* is the part of the wing proximal to the first and fifth digits, and the *hand wing* the part distal to the first and fifth digits.

The *wing-stroke angle*, ϕ , is defined as the angle between the straight lines uniting the shoulder joint and the wing tip when the wing tip is at the top and bottom of the stroke, respectively. The *stroke plane* is the plane in which these straight lines lie. The wing-tip path forms a compressed ellipse (Fig. 4), so a plane is a reasonable approximation.

KINEMATICS

In slow level flight, at a speed of 2–3 m s⁻¹, the long axis of the body is kept almost horizontal. In nine film sequences, the inclination of the stroke plane relative to the horizontal varied between 50° and 64° and averaged 57.8°.

Hovering flight differs in the following respects. The body is inclined, head up, at about 30° and the angle of tilt of the stroke plane is approximately 30° to the horizontal (Norberg, 1970a).

The wing-stroke angle is ca. 91° at a flight speed of ca. 2.35 m s⁻¹. The wing-beat frequency varies with the flight speed at the low speeds analysed. At 2.0 m s⁻¹ the wing-beat frequency is ca. 13.5 strokes s⁻¹, and at 3.0 m s⁻¹ ca. 10.0 strokes s⁻¹. In this limited speed interval a straight line seems to be a reasonable description of the functional relationship between wing-beat frequency and flight speed (Fig. 1). This regression line should not be extended outside this range, for in hovering flight the frequencies vary between 10.2 and 12.5 strokes s⁻¹ and do not fit the regression line.

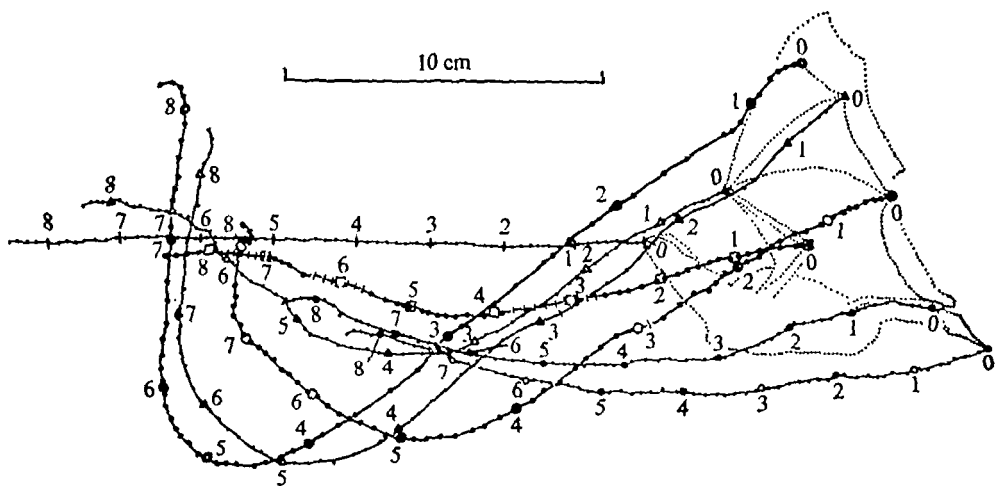


Fig. 2. Lateral projection of the tracks of uropatagium, ears, and different parts of the wings over a complete wing-stroke of *Plecotus auritus* flying horizontally at 2.35 m s^{-1} and with a stroke frequency of 11.9 Hz. The tracks are marked relative to the still air. During the upstroke the hand wing is brought vertically upwards relative to the still air. The numbers indicate each 100th of a second from the uppermost position of the wings. The positions, as traced from the frames, are indicated by small marks. ●, 3rd digit; ▲, 4th digit; ○, 5th digit; △, thumb; □, elbow; •, foot; ○, tail.

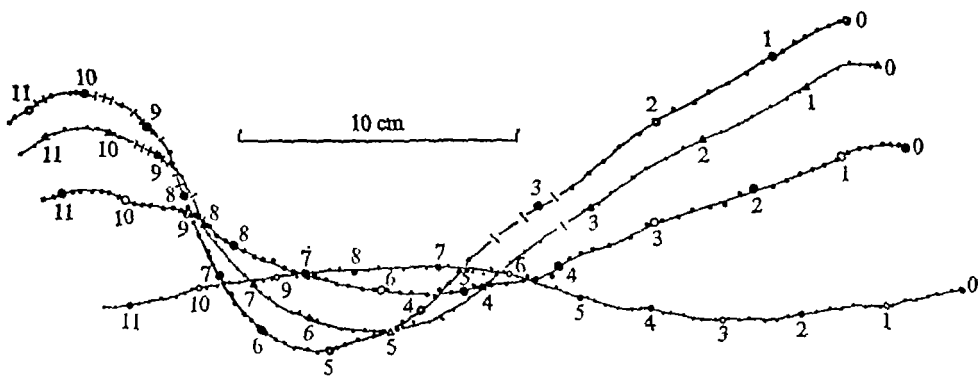


Fig. 3. Lateral projection of the wing movements of the bat flying at ca. 2.9 m s^{-1} and with a stroke frequency of 10.2 Hz. During the upstroke the wing-tip path is inclined upwards and forwards relative to the still air. Same symbols as in Fig. 2.

However, the stroke angle in hovering flight is ca. 120° , which is ca. 30° more than in horizontal flight ($V = 2.35 \text{ m s}^{-1}$).

The movements of the wings and tail membrane, uropatagium, in horizontal flight are shown in Figs. 2–13. The stroke of the wings (as extracted from Figs. 2 and 4, where $V = 2.35 \text{ m s}^{-1}$), is as follows: the downstroke (Figs. 6–8) starts with the wings extended at an angle of 49.4° above the horizontal. At the start the corresponding positional angle, γ , of the long wing-axis in the stroke plane is 153.5° . This positional angle, γ , is measured from the intersection below the bat between the wing-beat plane and a sagittal plane to the body through the wing hinge (Fig. 15). The wing then sweeps downwards and forwards fully extended and moves essentially in one plane,

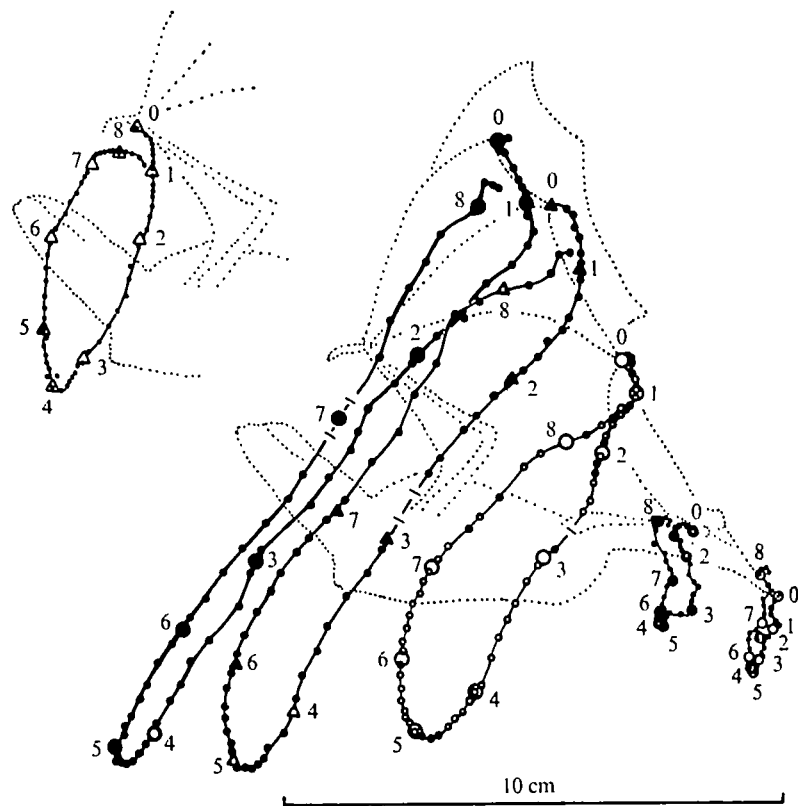


Fig. 4. Lateral projection of the same wing-stroke as in Fig. 2, but with the tracks traced relative to the shoulder joint and long axis of the body. The tail membrane (uropatagium) is moved down and up in synchrony with the wings. Same symbols as in Fig. 2.

tilted 58° to the horizontal. When the wing has reached an angle of 22.8° below the horizontal (positional angle $\gamma = 62.8^\circ$) the upstroke (Figs. 9 and 10) starts with a slight flexion at the elbow and wrist. The wrist begins to rise while the wing tip and trailing edge are still moving downwards (Figs. 2, 4, 11, 13). The whole wing is then brought upwards and backwards relative to the body. The hand wing is fully extended during the entire upstroke. The leading edge is kept rigid in the plane of the wing by a special arrangement of the second and third digits, which constitute a convex unit (Norberg, 1969).

At a flight speed of *ca.* 3 m s^{-1} , the wing-tip path has an upward-forward direction relative to the still air during the upstroke (Fig. 3). In slow flight (up to *ca.* 2 m s^{-1}) and in hovering, the wing-tip path is directed upwards and backwards relative to the still air during the upstroke. When extended during the later half of the upstroke, the wing then performs a backward and upward flick. At flight speeds of *ca.* $2-2\frac{1}{2} \text{ m s}^{-1}$, the wing is brought almost vertically relative to the still air during the upstroke (Fig. 2).

During the first half of the downstroke the wing is twisted, the middle and distal third being pronated (Table 1). Just before the wing reaches the horizontal level in the downstroke, at $\gamma = 90^\circ$, it begins to supinate (i.e. rotate nose-upwards). This rotation continues until the wing passes the horizontal level ($\gamma = 90^\circ$) in the upstroke, where it



Figs. 6-10. Long-eared bat *Plecotus auritus* in slow horizontal flight. Each plate contains three views of the same bat taken simultaneously with three cameras.

Fig. 6. Beginning of the downstroke. The tail and feet are held straight backwards.



Fig. 7. Middle of the downstroke. The twisting of the wings is clearly seen in the upper photograph.

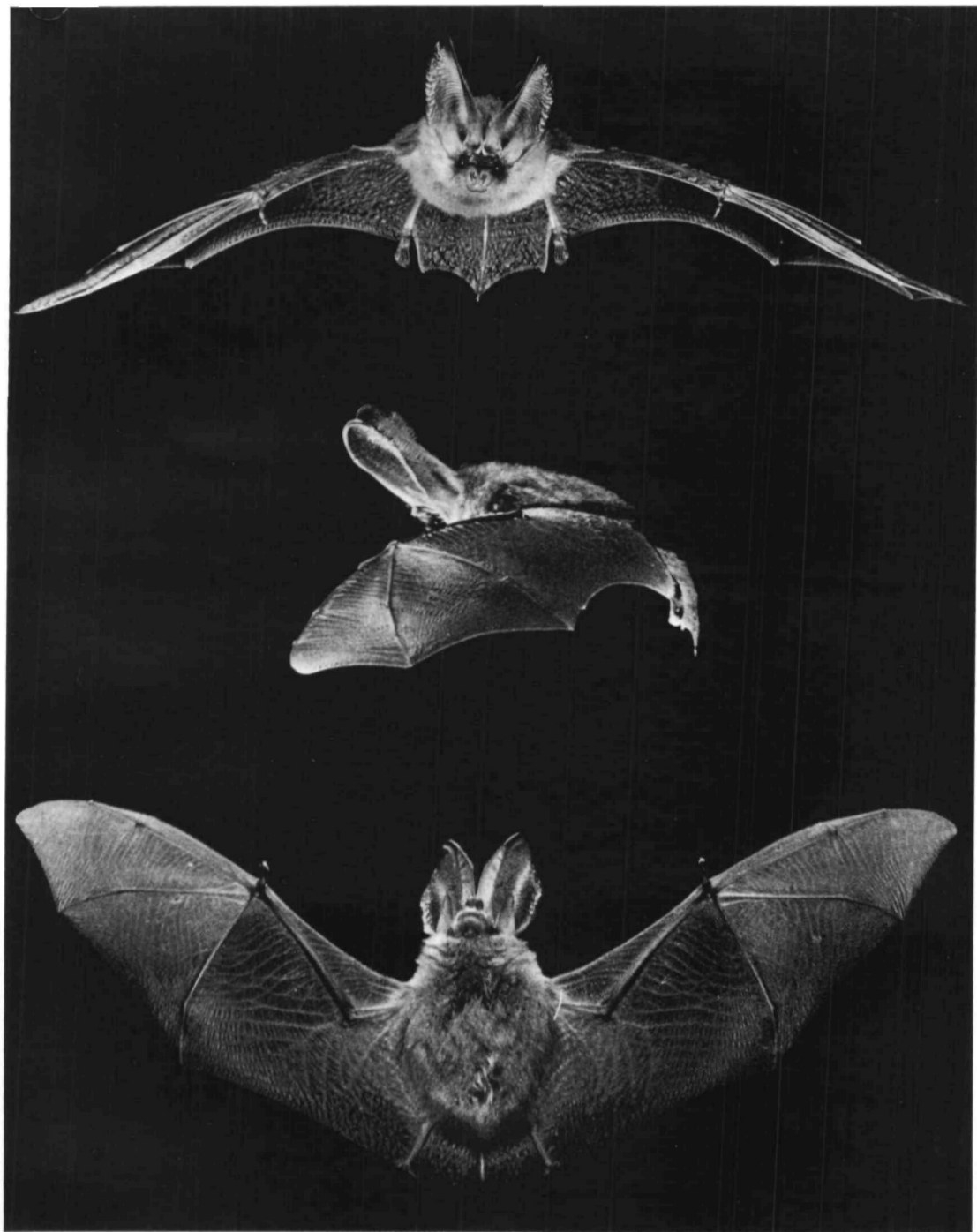


Fig. 8. Later part of the downstroke. The wings are sharply cambered, and the tail membrane is fully lowered.

ULLA M. NORBERG



Fig. 9. Beginning of the upstroke. The elbows and wrists are slightly flexed.
The camber is still pronounced.

ULLA M. NORBERG

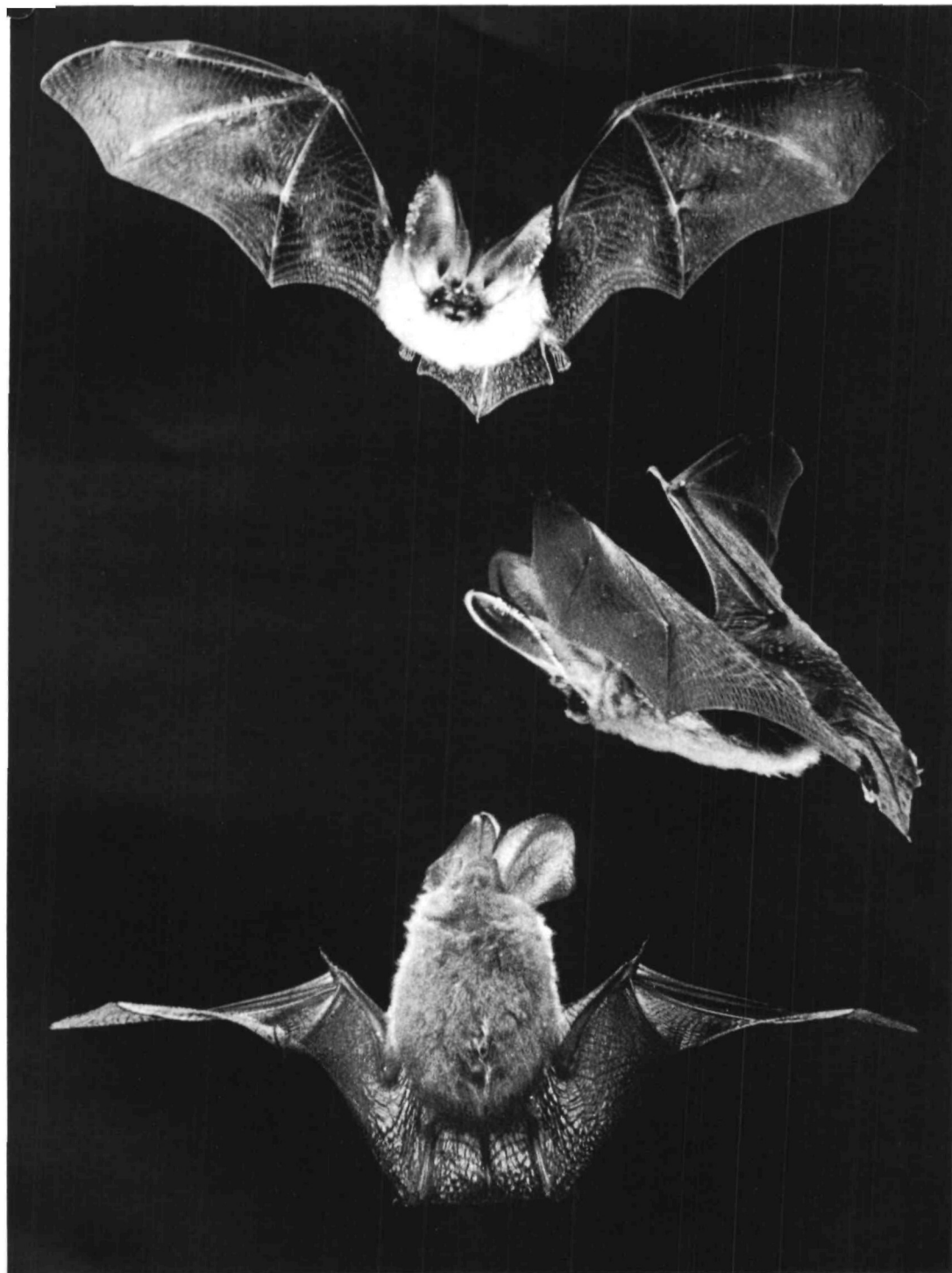


Fig. 10. Later part of the upstroke. The feet are raised which reduces the camber of the proximal part of the wings. The middle part is still cambered, but the wing tips are momentarily inverted.

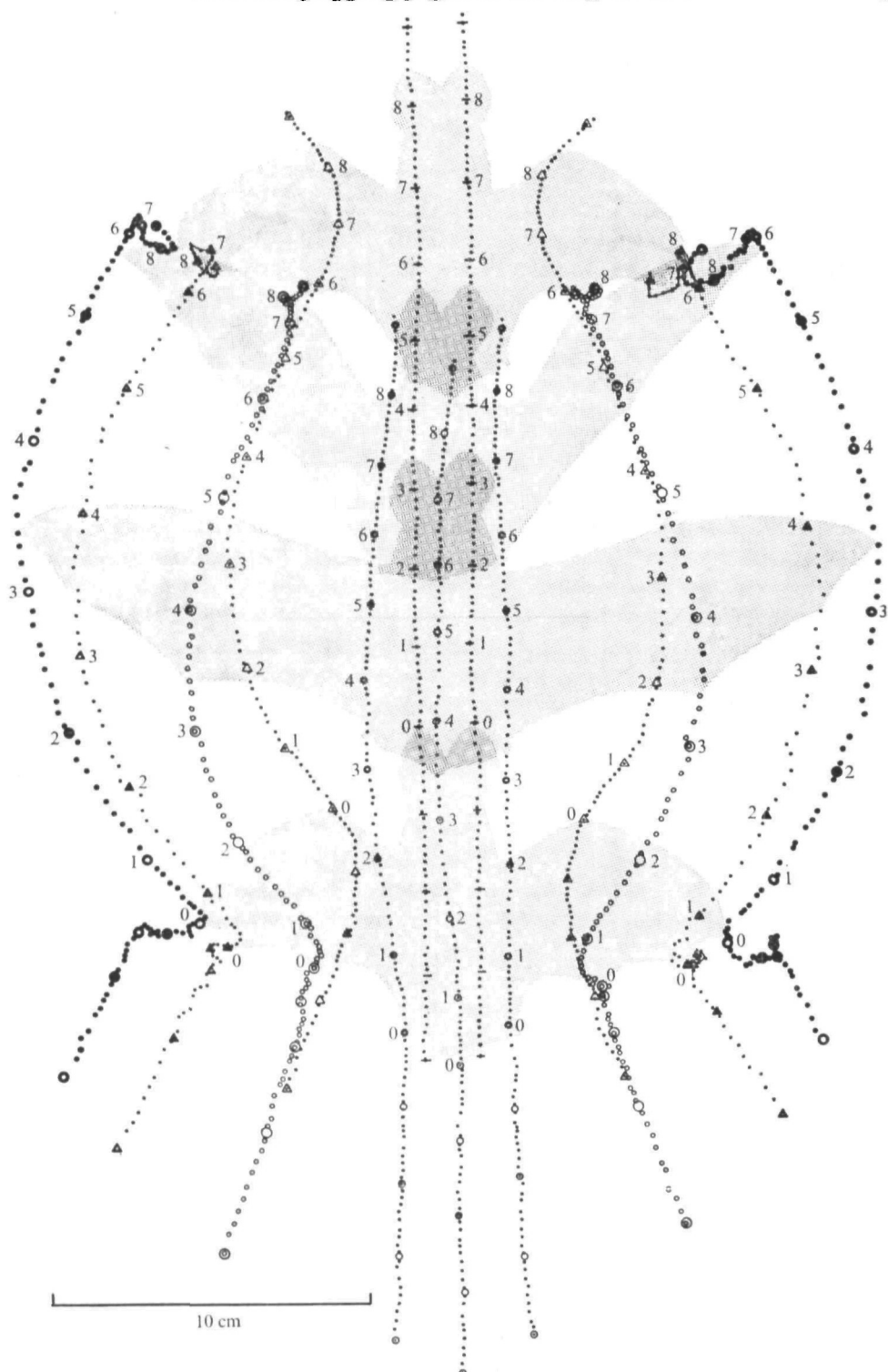


Fig. 5. Ventral projection of the wing movements of the bat flying at ca. 2.4 m s^{-1} and with a stroke frequency of 11.8 Hz. The tracks are marked relative to the still air. The wings are at the beginning of the downstroke at 0/100 s and again at 8.5/100 s a whole wing-stroke later. The downstroke is from 0/100 to 5.8/100 s (cf. Fig. 6), the upstroke from 5.8/100–8.5/100 s. During the upstroke the wings are brought vertically upwards relative to the still air (the first upstroke on the figure), or slightly backwards (the second upstroke, 7–8/100 s). Same symbols as in Fig. 2.

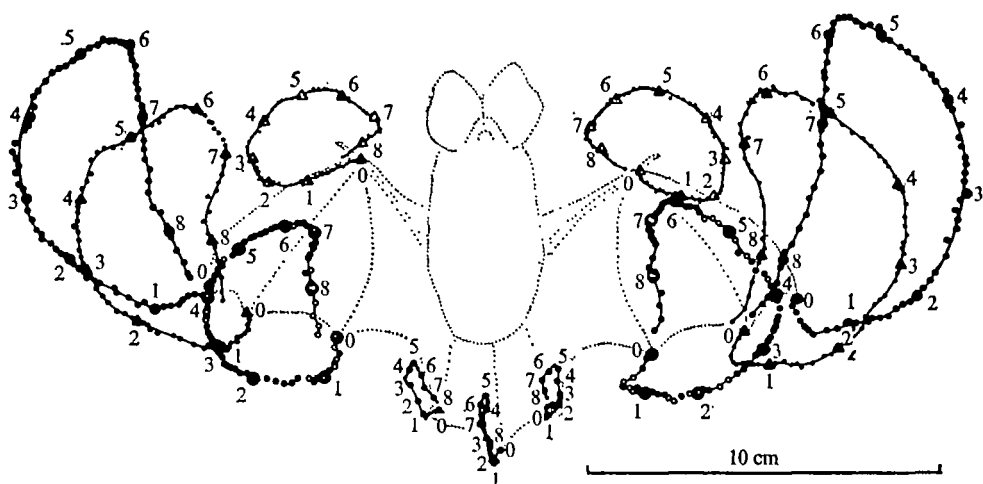


Fig. 11. The same wing-stroke as in Fig. 5, but with the tracks traced relative to the shoulder joint and long axis of the body. Same symbols as in Fig. 2.

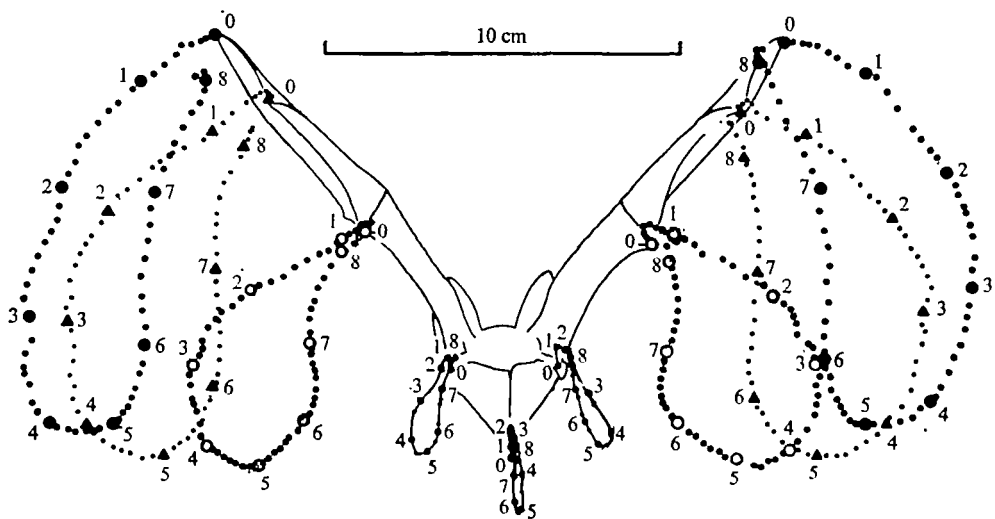


Fig. 12. Posterior projection of the wing movements. The movements of the feet and tail are clearly seen in this projection. Same symbols as in Fig. 2.

reverses the rotation. The wing is twisted during the upstroke with the distal part most supinated (Table 1). The nose-up rotation of the wing during the later half of the downstroke and the first half of the upstroke takes 32 ms and goes through 98° at $0.89R$ (strip 11) and through 64° at $0.57R$ (strip 7 = fifth digit). It thus occurs at angular velocities of 53.5 and 34.9 radians s⁻¹, respectively. In this rotation the inclination of the chord at $0.89R$ relative to the horizontal changes from 11° below the horizontal plane to 87° above the horizontal plane, and the chord at $0.57R$ from 4° below to 60° above the horizontal plane (Table 1, Fig. 14). The position of the lengthwise axis of rotation was determined at the level of the fifth digit, at $0.57R$. The wing

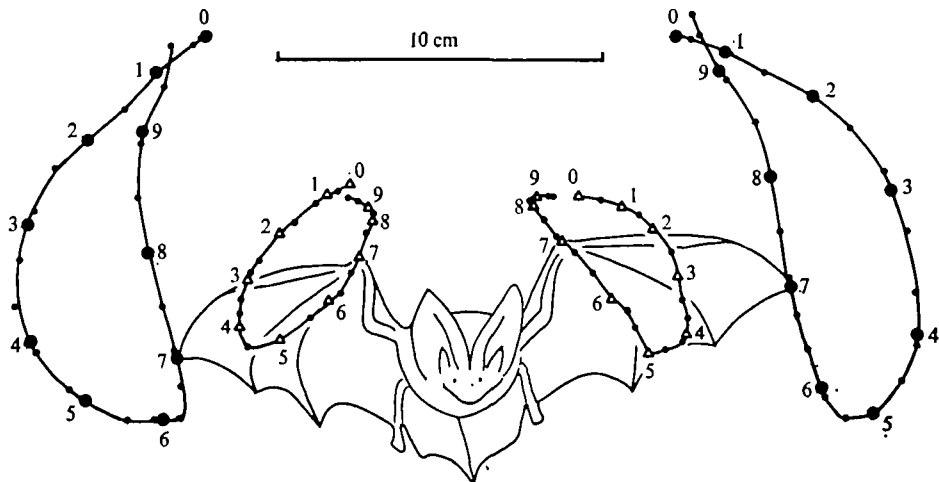


Fig. 13. Frontal projection of the wing movements. The tracks show that the wrists begin to rise (after ca. 45/100 s) before the wing tips have reached their bottom position. Same symbols as in Fig. 2.

Table 1. The chord angles (angles between wing chords and horizontal) at sections I-III (at strips 3, 7, and 11, respectively, defined in the text) for 14 various phases of the wing-stroke

Positional angle (γ) (deg.)	Time (ms)	Wing section			Upper reversal point
		I (deg.)	II (deg.)	III (deg.)	
153.5	0	6	2	-3	
145.0	11.0	8	-1	-8	
135.0	15.3	10	-1	-9	
110.0	24.0	12	-6	-13	
90.0	30.0	16	-5	-12	
85.0	32.0	19	-4	-11	
70.0	39.0	26	19	6	
65.0	45.0	32	35	37	
62.8	48.0	39	45	50	Lower reversal point
70.0	54.5	44	55	62	
90.0	64.0	38	60	87	
110.0	71.0	31	56	76	
125.0	76.0	24	37	48	
135.0	78.5	20	26	34	

here rotates around a point ca. 40 % of the chord length behind the leading edge. The chord at $0.24R$ (strip 3) does not rotate very much (Table 1).

At the level of the fifth digit the wing is positively cambered during the upstroke also. The feet are moved upwards during the upstroke, thereby reducing the positive chordwise camber of the proximal part of the wing. The wing membrane at the trailing edge bulges towards the morphological ventral side of the wing (Fig. 10, bottom) during the later half of the upstroke.

The movement of the long wing-axis is almost sinusoidal with respect to angular displacements about the humero-scapular joint, except during the last third of the upstroke. However, the deviation here from simple harmonic motion is small (Fig. 15).

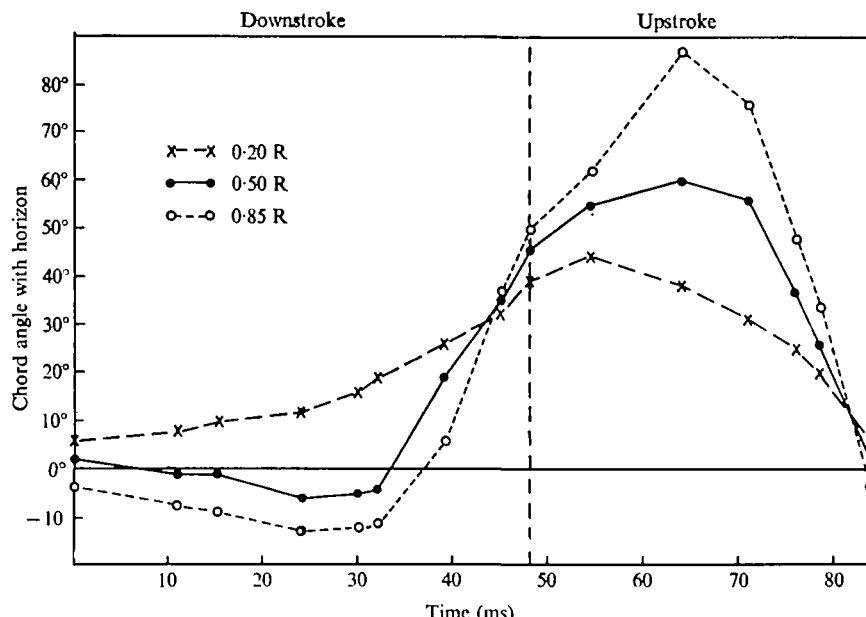


Fig. 14. Chord angles, relative to the horizontal, of three sections of the wing (at radial distance, $0.20R$ ($\times-\times$), $0.50R$ ($\bullet-\bullet$), and $0.85R$ ($\circ-\circ$), respectively, from the wing hinge), plotted against time, of the bat flying horizontally at ca. 2.35 m s^{-1} . Positive sign indicates nose-up orientation relative to the horizontal, negative sign nose-down orientation. Based on Figs. 2 and 5.

The maximum speed of the wing is reached in the middle parts of the down- and upstrokes at a positional angle of ca. 110° (i.e. above the horizontal). Both during the downstroke and upstroke the maximum speed amounts to ca. 7.3 m s^{-1} at wing tip. The relative speed of the wing at three sections ($0.20R$, $0.50R$ and $0.85R$) at a forward speed of $V = 2.35 \text{ m s}^{-1}$ is shown in Fig. 16.

The downstroke lasts ca. 52.6 % of the whole stroke time and the upstroke, therefore, 47.4 % ($N = 25$, S.D. = ± 3.02). The downstroke is here defined as the part of the stroke cycle when the wing tip is moving downwards although the wrist begins to rise before the tip has reached its bottom position. In the wing stroke analysed at a frequency of 11.9 s^{-1} , the downstroke lasted 48 ms and the upstroke 36 ms. However, the wrist began to rise ca. 10 ms before the wing tip. Thus, the downstroke of the wrist was 8 ms shorter than its upstroke.

The uropatagium moves down and up in synchrony with the wings. These movements are performed by the legs and tail and are shown in Figs. 2-5, 11 and 12.

FORCE COEFFICIENTS

General outline of the method. During flight with no vertical acceleration the vertical component of the aerodynamic resultant force must balance the weight of the flying animal. Similarly, with no horizontal acceleration, the horizontal component of the aerodynamic resultant force must balance the body drag. However, the force coefficients and the lift:drag ratio are unknown, and, hence, also the directions of the resultant force (F), and the sign of its components. But the directions of the lift (L)

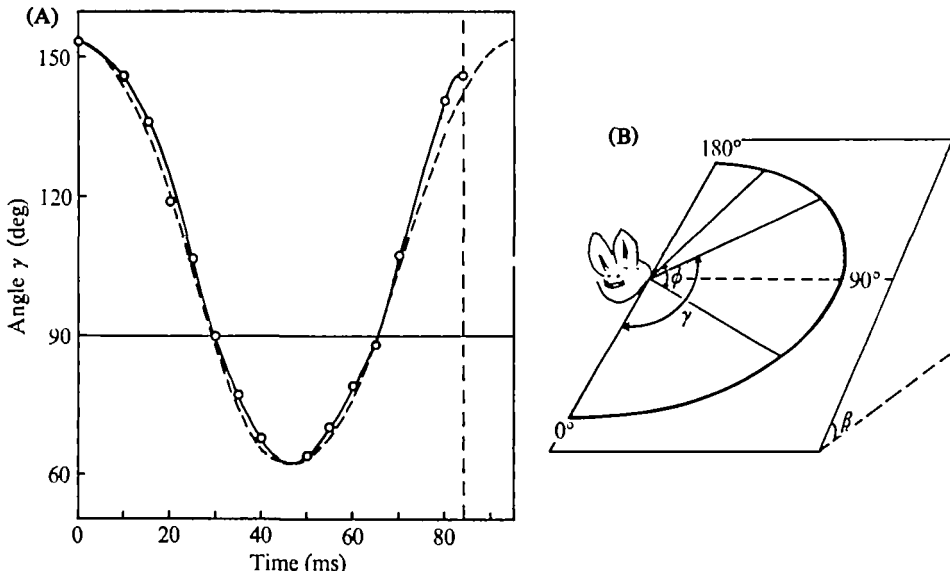


Fig. 15. (A) Comparison between the actual angular movements of the long wing-axis of the bat (full curve) and a sinusoidal movement (dashed curve). The long wing-axis is defined as an axis between the humero-scapular joint and the wing tip. The latter curve is calculated on the assumption that the wing-stroke is a simple harmonic motion. The agreement between the curve based on actual measurements and the calculated curve indicates that the wing performs essentially a simple harmonic motion. Since the wings are not raised to the same level as in the beginning of the downstroke in this wing-stroke, the period of the full curve is shorter than that of the dashed curve, which latter is twice the duration of the downstroke.

(B) Wing-stroke plane with a key to some of the symbols used. ϕ is the stroke angle of the wing (i.e. the total excursion angle of the wing) γ is the positional angle of the wing, measured in the stroke plane from the intersection below the bat between the stroke plane and a sagittal plane to the body through the wing hinge. β is the inclination of the stroke plane relative to the horizontal.

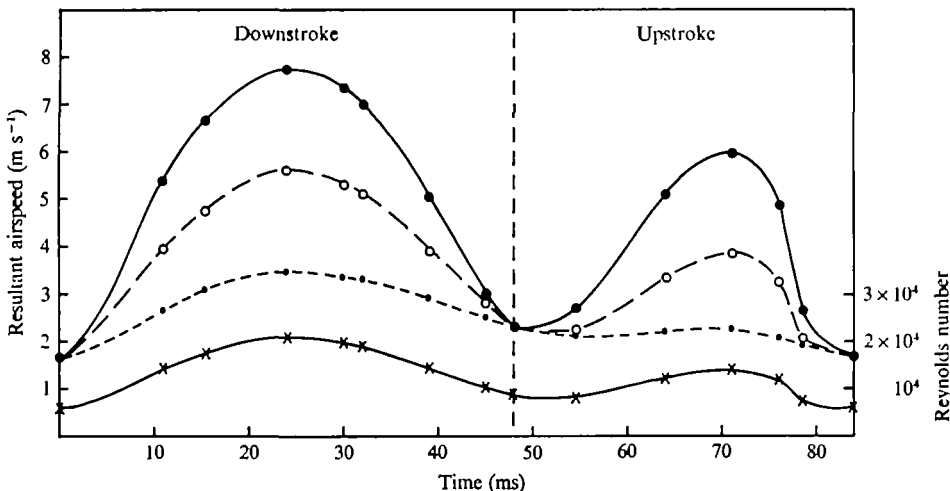


Fig. 16. Resultant airspeed for three sections of the wing (●—● : $0.20R$, ○—○ : $0.50R$, ●—○ : $0.85R$) plotted against time, and corresponding Reynolds number (×—×) at $0.85R$ (right ordinate). The resultant air speed is the vector sum of the flapping velocity, the induced velocity, and the projection of the forward flight speed to a plane normal to the long wing-axis.

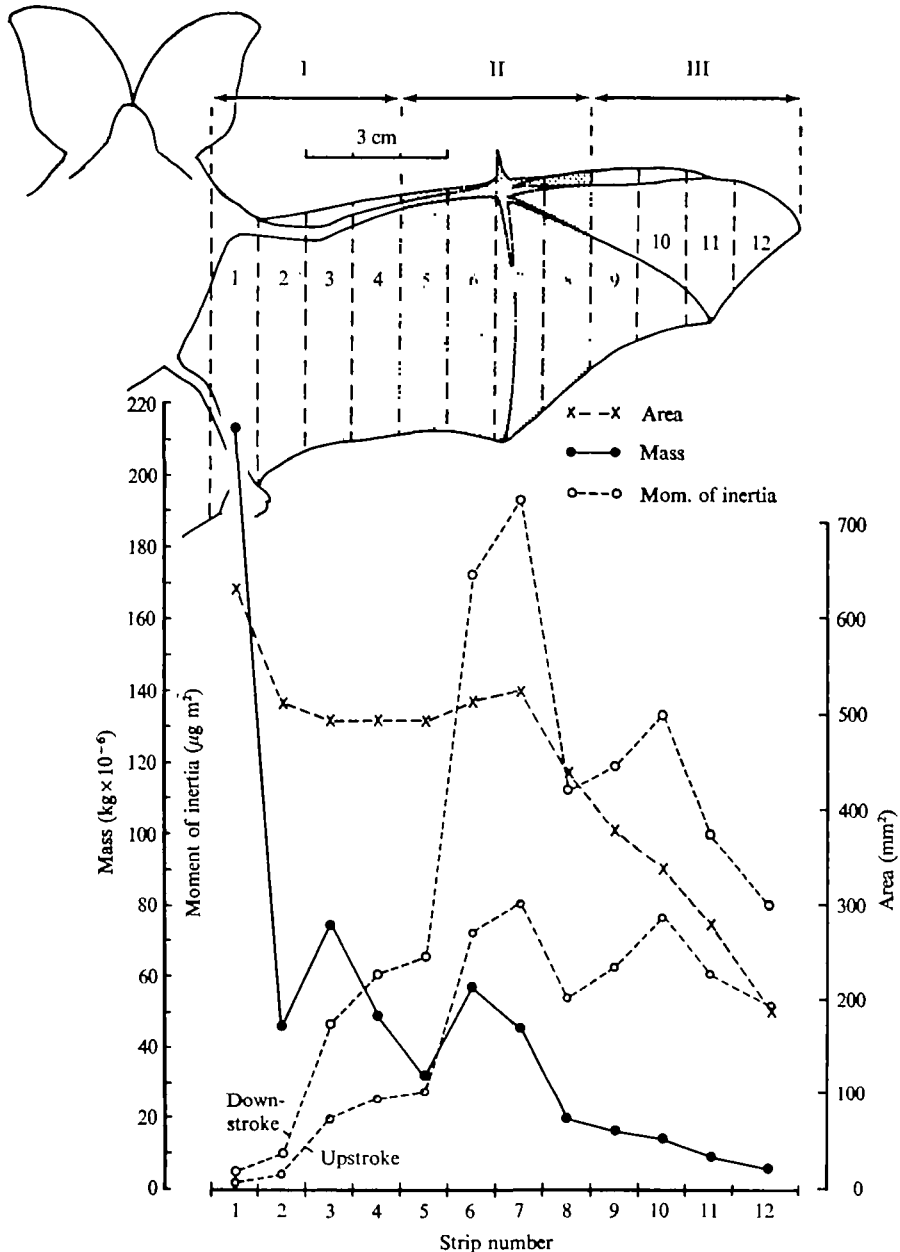


Fig. 17. Spanwise distribution of area, mass, and moment of inertia of the wing. Values given for 12 chordwise strips of the wing. The difference between the downstroke and upstroke curves for the moment of inertia is due to flexion of the wing during the upstroke.

and drag (D) forces (but not the magnitudes) can be found, since the direction of the resultant relative airstream can be estimated. Therefore, the vertical and horizontal components of the *lift* and *drag* forces are used instead to estimate the vertical and horizontal forces, respectively. Thus, the sum of the vertical components of the *lift* and *drag* forces (as integrated over a whole wing-stroke and over the whole wings)

Table 2. Weight and wing measurements of
Plecotus auritus used in calculations

Body weight, W	0.0883 N
Wing length, R	0.124 m
Wing span, b	0.270 m
Wing area, A	0.0123 m ²
Area of one wing	0.0053 m ²
Uropatagium area	0.0015 m ²
Wing loading, W/A	7.18 N m ⁻²
Aspect ratio, b^2/A	5.9
Flight muscle mass/body mass	0.137*

* Data from Betz (1958).

Table 3. Flight parameters used in calculations

Forward speed, V	2.35 m s ⁻¹
Induced wind, V_i	0.27 m s ⁻¹
Stroke angle, ϕ	90.7° = 1.58 rad
Stroke frequency, n	11.9 s ⁻¹
Angle of tilt of stroke plane, β	58°
Air density, ρ	1.22 kg m ⁻³

must equal the weight of the bat as integrated over the same time. In the same way the integral of the horizontal components of the *lift* and *drag* forces must equal the integral of the body drag of the bat.

To use an equation system with the vertical and horizontal components of the *lift* and *drag* forces is a novel way of finding the lift and drag coefficients and, thus, their ratio.

Calculations. The wing was divided transversely into three sections, comprising strips 1–4 (section I), 5–8 (section II), and 9–12 (section III), respectively (Fig. 17). The inclination of the chords and airflow velocities were measured for the middle of strips 3, 7, and 11. These strips are regarded to be representative of wing sections I, II, and III, respectively. Data were taken from a representative stroke during unaccelerated (as judged from the film) horizontal flight (Figs. 2 and 4, Tables 2 and 3). Only movement components normal to the long wing-axis are taken into account.

The movement of the long wing-axis is almost sinusoidal with respect to angular displacement, except during the last third of the upstroke (Fig. 10). During the down-stroke and two-thirds of the upstroke the angular movement then is

$$\gamma(t) = \bar{\gamma}(t) + \frac{1}{2}\phi \sin(2\pi nt), \quad (1)$$

where γ is the positional angle of the long wing-axis in the stroke plane, $\bar{\gamma}(t)$ is the mean positional angle, ϕ is the stroke angle, t is time, and n is the wing-stroke frequency. The angular velocity is

$$d\gamma(t)/dt = \pi\phi n \cos(2\pi nt). \quad (2)$$

The flapping velocity of a wing-element at distance r from the fulcrum is

$$v(r, t) = r d\gamma(t)/dt = r\pi\phi n \cos(2\pi nt). \quad (3)$$

The flapping velocity in the last third of the upstroke is based on data from the film.

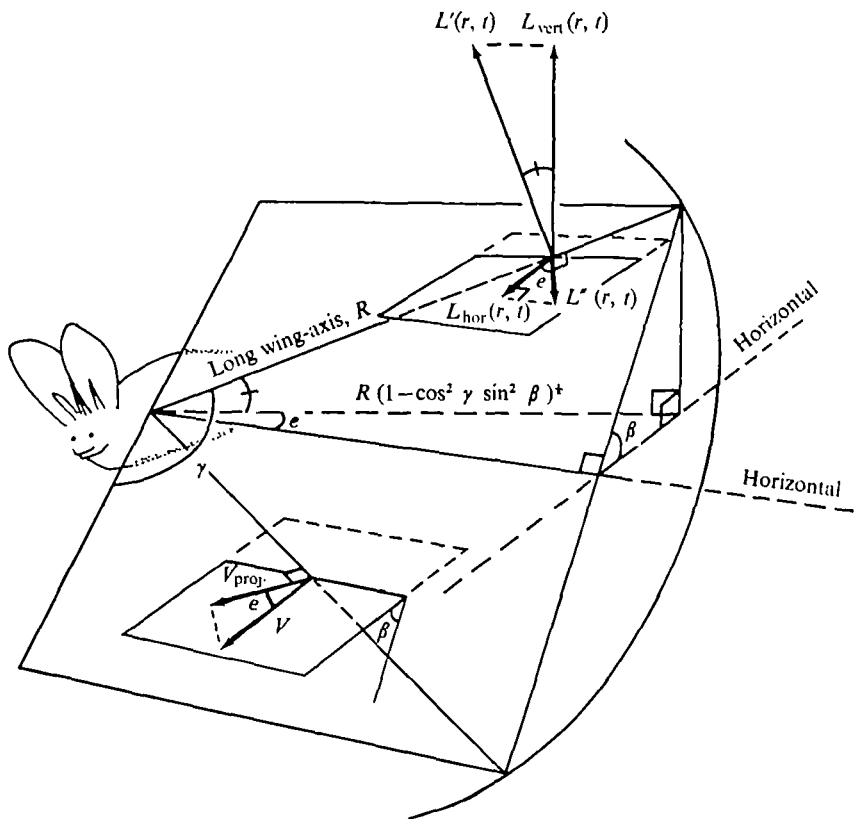


Fig. 18. Diagram showing the component, $L'(r, t)$, of the instantaneous lift force in a plane normal to the long wing-axis, and its vertical projection, $L_{ver}(r, t)$. β is the inclination of the stroke plane relative to the horizontal, γ the positional angle, and e the angle between a plane normal to the long wing-axis and the flight path. V_{proj} is the projection of the forward speed, V , to this plane.

The instantaneous resultant velocity, $V_R(r, t)$, is the resultant of three speed components (namely the flapping speed, the induced velocity, V_i , and the projection, $V_{proj}(r, t)$, of the forward speed, V , to a plane normal to the long axis of the wing).

The induced velocity is assumed to be constant along the wing during the entire wing-stroke, though there might be fluctuations in the down- and upstrokes. According to the momentum theorem for an ideal actuator disc, the induced velocity, V_i , at the level of the disk, is obtained from the formula

$$V_i(V^2 + V_i^2)^{\frac{1}{2}} = \frac{W}{S_d \cdot 2\rho}, \quad (4)$$

where V is the forward speed, W is the weight, S_d is the disc area, and ρ is the air density. The disc area is taken to be

$$S_d = \frac{1}{4}\pi b^2, \quad (5)$$

where b is the wing span.

The projection, $V_{proj}(t)$, of the forward speed, V , to planes normal to the long axis

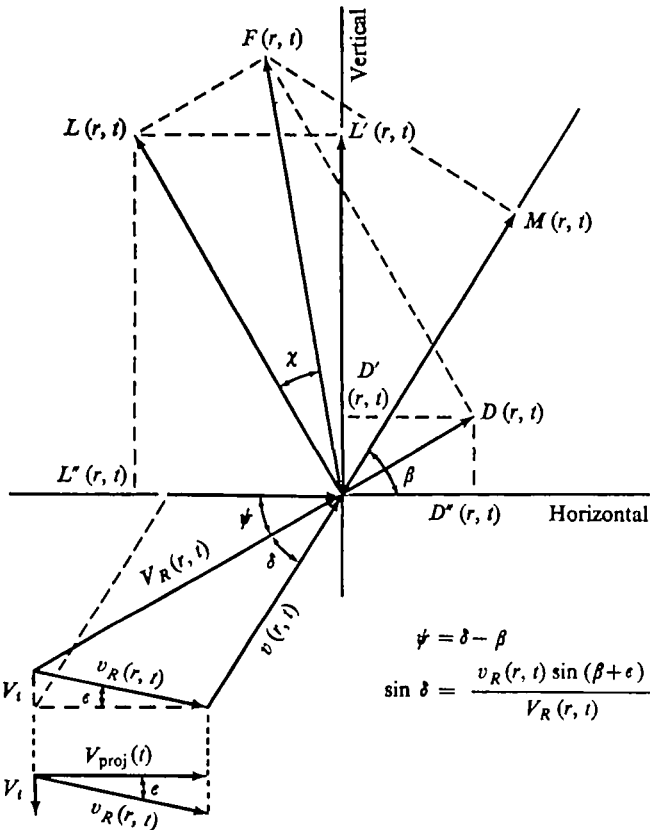


Fig. 19. Velocities at, and forces acting on, a chordwise wing-segment at a distance r from the fulcrum during the downstroke in horizontal flight. See text for further explanation.

of the wing equals $V \cdot \cos \epsilon$, where ϵ is the angle between this plane and the flight path (Fig. 18). Further, $\cos \epsilon$ is calculated by the expression

$$\cos \epsilon = \left(\frac{1 - \cos^2 \gamma}{1 - \cos^2 \gamma \sin^2 \beta} \right)^{\frac{1}{2}}. \quad (6)$$

Fig. 19 shows that the resultant $v_R(r, t)$ of $V_{\text{proj}}(t)$ and V_t is

$$v_R(r, t)^2 = V_{\text{proj}}(t)^2 + V_t^2, \quad (7)$$

and

$$\tan \epsilon = \frac{V_t}{V_{\text{proj}}(t)}. \quad (8)$$

The resultant airspeed $V_R(r, t)$ during the downstroke then is

$$V_R(r, t)^2 = v(r, t)^2 + v_R(r, t)^2 + 2v(r, t)v_R(r, t) \cos(\beta + \epsilon), \quad (9)$$

and during the upstroke

$$V_R(r, t)^2 = v(r, t)^2 + v_R(r, t)^2 - 2v(r, t)v_R(r, t) \cos(\beta + \epsilon), \quad (10)$$

where β is the angle of tilt of the stroke plane relative to the horizontal.

The instantaneous lift and drag forces produced by the three chordwise sections of the wing are

$$L(r, t) = \frac{1}{2} \rho \cdot V_R(r, t)^2 \cdot A'(r) \cdot C_L(r, t), \quad (11)$$

and

$$D(r, t) = \frac{1}{2} \rho \cdot V_R(r, t)^2 \cdot A'(r) \cdot C_D(r, t), \quad (12)$$

where $A'(r)$ are the areas of sections I-III at distance r from fulcrum, and $C_L(r, t)$ and $C_D(r, t)$ are the instantaneous coefficients of lift and drag, respectively.

As the lift:drag ratio is unknown, the direction of the resultant force, $F(r, t)$ cannot be calculated. However, the directions of $L(r, t)$ and $D(r, t)$ are known. The sum of the vertical components of $L(r, t)$ and $D(r, t)$ equals the vertical component of $F(r, t)$, and the sum of the horizontal components of $L(r, t)$ and $D(r, t)$ equals the horizontal component of $F(r, t)$.

The components of $L(r, t)$ and $D(r, t)$ in the vertical plane through the long wing-axis and normal to the long wing-axis are:

$$L'(r, t) = L(r, t) \cos \psi \quad (13)$$

and

$$D'(r, t) = D(r, t) \sin \psi. \quad (14)$$

Angle $\psi = \delta - \beta$ during the downstroke and $\psi = \pi - (\delta + \beta)$ (15, 16)

during the upstroke, where

$$\sin \delta = \frac{v_R(r, t) \sin(\beta + \epsilon)}{V_R(r, t)} \quad (17)$$

(Fig. 19). Then the vertical components of these forces are

$$L_{\text{vert}}(r, t) = L'(r, t) (1 - \cos^2 \gamma \sin^2 \beta)^{\frac{1}{2}} \quad (18)$$

and

$$D_{\text{vert}}(r, t) = D'(r, t) (1 - \cos^2 \gamma \sin^2 \beta)^{\frac{1}{2}} \quad (19)$$

which can be seen from Fig. 18.

The horizontal components normal to the long wing-axis of $L(r, t)$ and $D(r, t)$ are

$$L''(r, t) = L(r, t) \sin \psi \quad (20)$$

and

$$D''(r, t) = D(r, t) \cos \psi. \quad (21)$$

The components of these forces in the direction of the flight path are then

$$L_{\text{hor}}(r, t) = L''(r, t) \cos e = L''(r, t) \left(\frac{1 - \cos^2 \gamma}{1 - \cos^2 \gamma \sin^2 \beta} \right)^{\frac{1}{2}}, \quad (22)$$

$$D_{\text{hor}}(r, t) = D''(r, t) \cos e = D''(r, t) \left(\frac{1 - \cos^2 \gamma}{1 - \cos^2 \gamma \sin^2 \beta} \right)^{\frac{1}{2}}. \quad (23)$$

The sum of the vertical components of the lift and drag forces of the two wings (each with N strips), integrated over a complete stroke cycle of time duration T , equals the weight of the bat integrated over the same time, and is

$$\int_{t=0}^{t=T} W dt = \int_{t=0}^{t=T} \left[\sum_{r=1}^{r=N} (L_{\text{vert}}(r, t) + D_{\text{vert}}(r, t)) \right] dt. \quad (24)$$

The horizontal components of the lift and drag forces of the two wings integrated

over a complete stroke cycle equals the body drag, D_b , integrated over the same time, and is

$$\int_{t=0}^{t=T} D_b dt = \int_{t=0}^{t=T} \left[\sum_{r=1}^{r=N} (L_{\text{hor}}(r, t) + D_{\text{hor}}(r, t)) \right] dt. \quad (25)$$

The body (or parasite) drag is proportional to the frontal (cross-sectional) area of the body, and to the square of the forward speed, or

$$D_b = \frac{1}{2} \rho A_e V^2, \quad (26)$$

where A_e is the equivalent flat plate area of the body. It is the greatest frontal area, multiplied by its drag coefficient (Pennycuick, 1972). It can be measured in a wind tunnel on a frozen body, but can also be estimated from the formula

$$A_e = (6.2 \times 10^{-4}) W^{2/3} \quad (27)$$

(Pennycuick, 1972). The body drag coefficient is assumed to be 0.43, and this is built into the formula. To this area, the frontal area of the ears must be added. Then

$$D_b = \frac{1}{2} \rho (A_e + A_{\text{ear}}) V^2. \quad (28)$$

The ears are assumed to have a drag coefficient of 1 like a flat plate transverse to the airflow.

Summarizing, by setting up the following equation system, the values of C_L and C_D , as averaged over the whole wing and whole wing-stroke, can be solved:

$$\begin{aligned} \int_{t=0}^{t=T} W dt &= C_L \int_{t=0}^{t=T} \left[\sum_{r=1}^{r=N} \frac{1}{2} \rho V_R(r, t)^2 A'(r) (\cos \psi) (1 - \cos^2 \gamma \sin^2 \beta)^{\frac{1}{2}} \right] dt \\ &\quad + C_D \int_{t=0}^{t=T} \left[\sum_{r=1}^{r=N} \frac{1}{2} \rho V_R(r, t)^2 A'(r) (\sin \psi) (1 - \cos^2 \gamma \sin^2 \beta)^{\frac{1}{2}} \right] dt, \end{aligned} \quad (29)$$

$$\begin{aligned} \int_{t=0}^{t=T} D_b dt &= C_L \int_{t=0}^{t=T} \left[\sum_{r=1}^{r=N} \frac{1}{2} \rho V_R(r, t)^2 A'(r) (\sin \psi) \left(\frac{1 - \cos^2 \gamma}{1 - \cos^2 \gamma \sin^2 \beta} \right)^{\frac{1}{2}} \right] dt \\ &\quad + C_D \int_{t=0}^{t=T} \left[\sum_{r=1}^{r=N} \frac{1}{2} \rho V_R(r, t)^2 A'(r) (\cos \psi) \left(\frac{1 - \cos^2 \gamma}{1 - \cos^2 \gamma \sin^2 \beta} \right)^{\frac{1}{2}} \right] dt. \end{aligned} \quad (30)$$

Procedure and results. The areas of the sections I-III were obtained from addition of the narrower strip areas (of strips 1-4, 5-8, and 9-12, respectively). During the up-stroke, the area of the wing is reduced by flexion at the elbow and wrist. The area of the arm wing (strips 1-6) was estimated to be reduced to ca. 65 % of its area when extended, while the area of the hand wing (strips 7-12) was not reduced at all. At the reversal points an area of 80 % of the area of the arm wing, when extended, was used. For the hand wing the entire area was included. The values of the radii used in calculations were reduced correspondingly.

It was somewhat difficult to measure the inclination of the wing chords for the different strips. For strips 3, 7, and 11, however, there are some reference points (for example, the thumb and finger tips) to use, and these strips were considered to be representative for the proximal (section I), middle (section II), and distal (section III) parts, respectively, of the wing. The inclinations of the chords for these strips were estimated from Figs. 2 and 5. The effective radii of gyration of the three sections

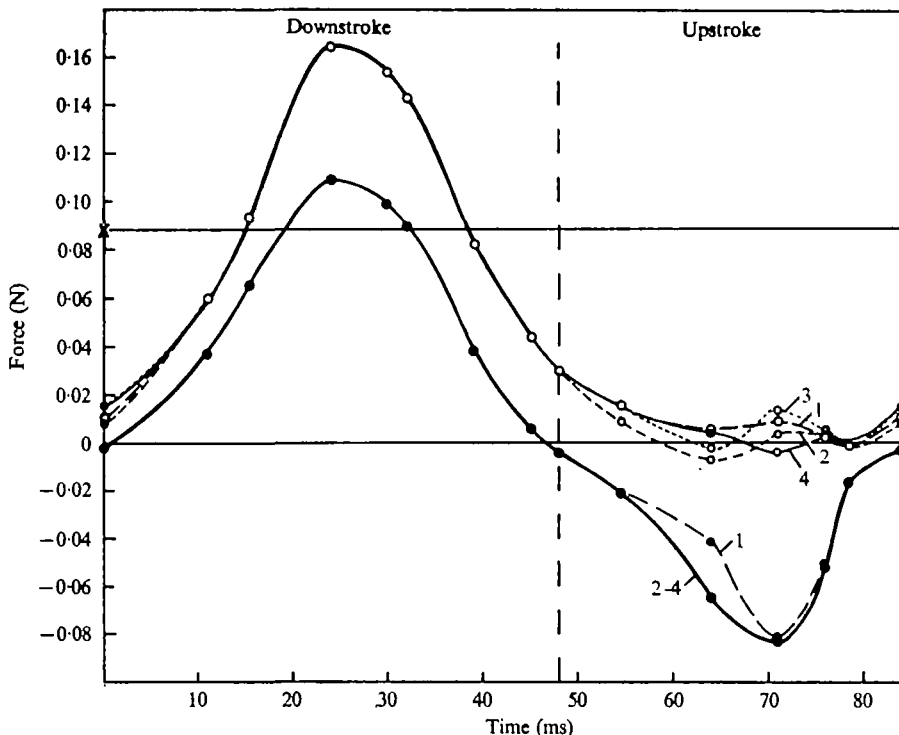


Fig. 20. The virtual force indices, L_{vert}/C_L ($\circ-\circ$) and D_{vert}/C_D ($\bullet-\bullet$), for the vertical components of the lift and drag forces, respectively, plotted against time. The area under the L_{vert}/C_L -curve, multiplied by the lift coefficient, plus the area under the D_{vert}/C_D -curve, multiplied by the drag coefficient, must equal the body weight of the bat as integrated over the whole wing-stroke. The weight is indicated by a cross on the ordinate. Four different cases are shown, and are discussed in the text.

agree approximately with the radii of these three strips (i.e. the distance from the fulcrum to the middle of the respective strip).

The virtual force indices, L_{vert}/C_L , D_{vert}/C_D , L_{hor}/C_L , and D_{hor}/C_D , respectively, were estimated for 14 positions of the wings during the wing-stroke and for each of the three sections. By integrating the summed curves for all sections of both wings with respect to the time for a whole wing-stroke, the integrated values of the indices were found. Using equations (29) and (30), the values of C_L and C_D , as averaged over a whole wing-stroke, were obtained. The area under the summed L_{vert} index curve, multiplied by the lift coefficient plus the area under the summed D_{vert} index curve, multiplied by the drag coefficient, must equal the body weight as integrated over the whole wing-stroke (Fig. 20). The area under the summed L_{hor} index curve, multiplied by the lift coefficient, plus the area under the summed D_{hor} index curve, multiplied by the drag coefficient, must equal the body drag (Fig. 21).

To know the sign of the angle ψ , one has to know if the angle of attack (i.e. the angle between the direction of the airflow and wing's zero-lift line) is positive or negative. One also must know the direction of the resultant, relative, airflow.

The zero-lift lines are difficult to determine. They change during the wing-stroke, especially during the upstroke, as a consequence of the changes of the wing profile.

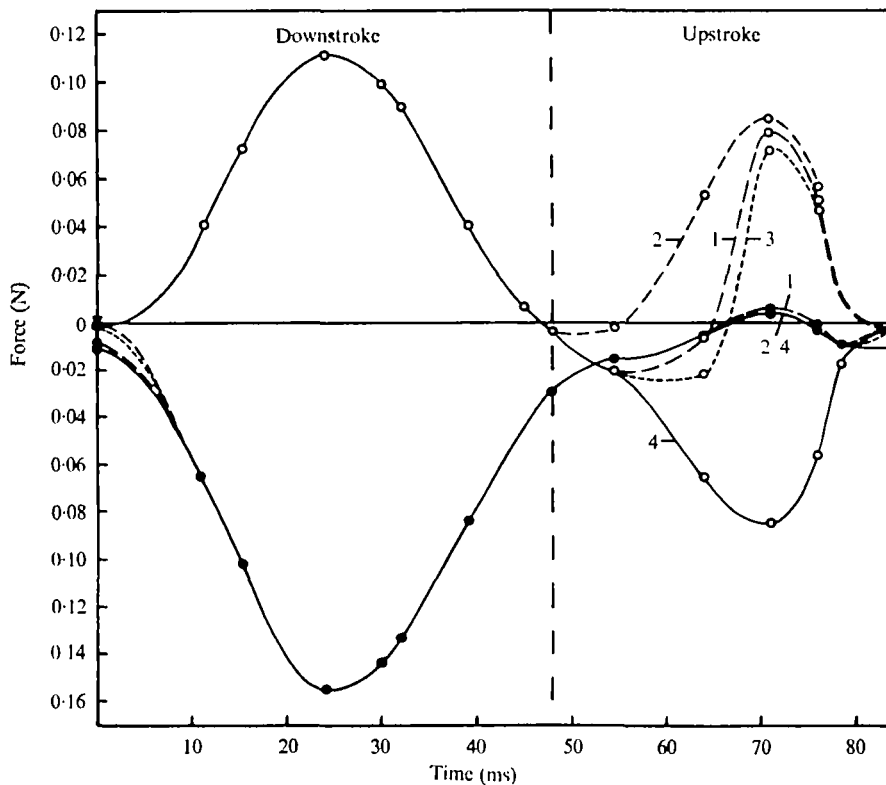


Fig. 21. The virtual force indices, L_{hor}/C_L and D_{hor}/C_D , for the horizontal components of the lift and drag forces, respectively, plotted against time. The area under the L_{hor}/C_L -curve ($\circ-\circ$), multiplied by the lift coefficient, plus the area under the D_{hor}/C_D -curve, ($\bullet-\bullet$), multiplied by the drag coefficient, must equal the body drag of the bat as integrated over the whole wing-stroke. The body drag is shown by a cross on the ordinate ($D_b \approx 0.00105$ N). Four different cases are shown, and are discussed in the text.

Pennycuick (1973) estimated the positions of the zero-lift lines of the wings of *Rousettus aegyptiacus* in gliding flight in wind tunnel experiments (using formulae given by Pankhurst (1944) and Abbott & Doenhoff (1959)). He found that the zero-lift angle (the angle between the wing chord and zero-lift line) varied between 10.5° and 21.3° for different sections of the wing. Using Pennycuick's result, the four following alternative sets of assumptions were used to calculate the lift forces elicited during the upstroke.

(1) Airflow angles (the angles between the directions of airflow and wing chords) between -10° and -22° are considered to be so close to the zero-lift angles, that no lift forces are obtained at these angles (marked ± 0 in Table 4).

(2) Airflow angles $\leq -10^\circ$ are negative angles of attack. Lift forces are then elicited in the direction of the morphological ventral side of the wing.

(3) Airflow angles $\leq -22^\circ$ are negative angles of attack.

(4) All angles of attack are positive during the entire wing-stroke. This is probably not true, but gives a maximum, potential value of the lift:drag ratio.

The drag forces of the wings are assumed to be equal in alternatives 2-4, though the drag coefficients decrease with decreasing angle of attack. However, this assumption

Table 4. Airflow angles relative to the wing chord and signs of angles of attack for sections I-III (for strips 3, 7, and 11, respectively) of the wing

(Zero-lift line is assumed to lie between -10° and -22° . This means that angles of attack between -10° and -22° are assumed to lie so close to the zero-lift line that no lift force is generated. These angles are denoted ± 0 , implying no lift. +, positive angle of attack; -, negative angle of attack.)

Positional angle (γ) (deg.)	Time (ms)	I		II		III		Upper reversal point
		(deg.)	(deg.)	(deg.)	(deg.)	(deg.)	(deg.)	
153.5	0	-3 +		-7 +		-12	± 0	
145.0	11.0	23 +		31 +		31	+	
135.0	15.3	29 +		34 +		32	+	
110.0	24.0	32 +		29 +		28	+	
90.0	30.0	34 +		29 +		29	+	
85.0	32.0	37 +		29 +		30	+	Downstroke
70.0	39.0	36 +		44 +		39	+	
65.0	45.0	32 +		43 +		52	+	
62.8	48.0	31 +		38 +		42	+	Lower reversal point
70.0	54.5	19 +		4 +		-9	+	
90.0	64.0	-7 +		-22 ± 0		-10	± 0	
110.0	71.0	-21 ± 0		-33 -		-25	-	Upstroke
125.0	76.0	-22 ± 0		-47 -		-49	-	
135.0	78.5	-8 +		-29 -		-41	-	

Table 5. Average lift and drag coefficients and lift:drag ratios in horizontal flapping flight at a speed V of 2.35 m s^{-1} (they are calculated according to four alternative sets of states of wing function as described and discussed in the text)

Alt.	C_L	C_D	L/D
1	1.4	0.9	1.6
2	1.4	1.2	1.2
3	1.4	0.9	1.6
4	1.6	0.4	4.0

results in an average C_D . When the lift forces in alternatives 1 are set to zero, the corresponding drag forces are not zero but assumed to be reduced to 60%. This assumption is based on Pennycuick's (1971) wind-tunnel studies on *Rousettus* in gliding flight. The virtual force index curves for the four alternatives are shown in Figs. 20 and 21.

During the downstroke the angle of attack is positive at all different sections and phases (Table 4). It is not so easy, however, to determine when the angle of attack is positive and when it is negative during the upstroke. It can be seen from Figs. 9 and 10 that the fifth digit is somewhat flexed during the upstroke, thereby highly cambering (anteroposteriorly) the middle section of the wing in the positive sense. During the middle part of the upstroke the trailing edge of the hand wing is cambered in the negative sense (bulging towards the morphological ventral side of the wing, Fig. 10), indicating a negative angle of attack at this part of the wing. This supports the first alternative.

The result of the calculations of lift and drag coefficients with the four alternative assumptions (above) is listed in Table 5. The lift coefficients do not vary much in the

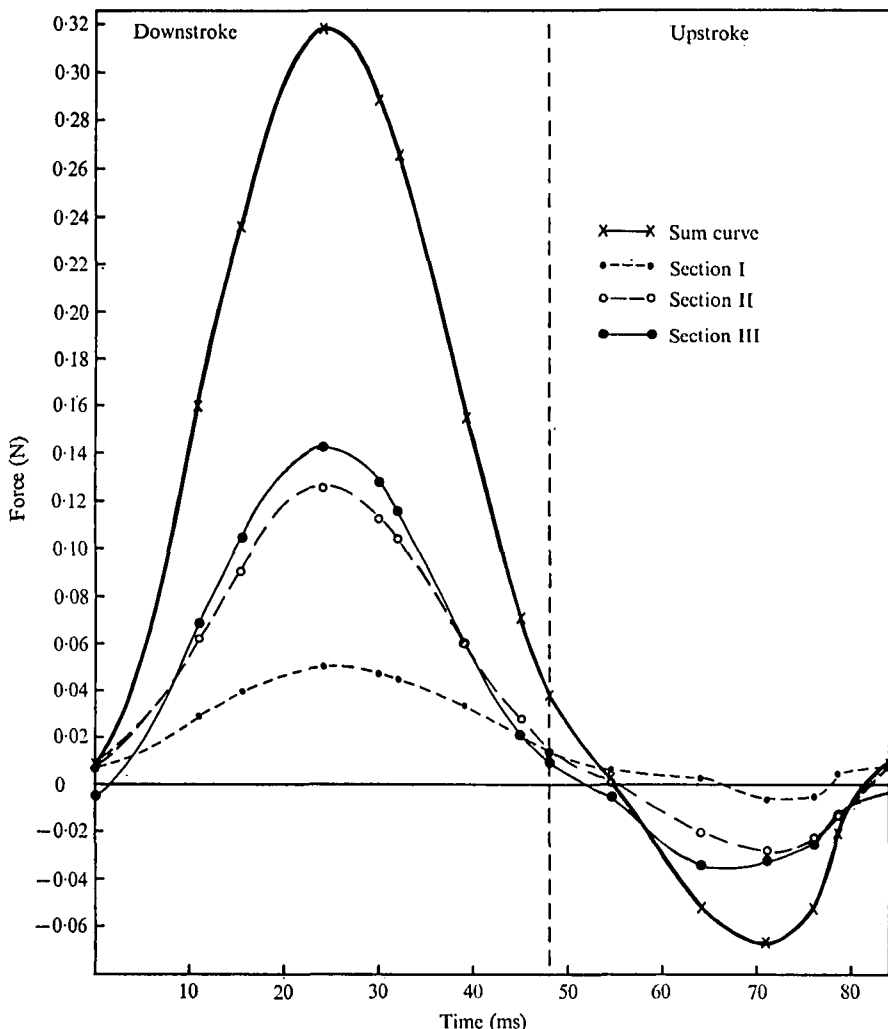


Fig. 22. Curves showing the sum of the vertical projections of the virtual lift and drag forces, plotted against time for three sections of the wing (proximal, middle, and distal part, as indicated in Fig. 17). The summed curve for the three wing sections is also shown. Calculations based on alternative 1 (described and discussed in the text) involving a C_L value of 1.4 and a C_D value of 0.9.

four alternatives, and lie between 1.4 and 1.6. However, the drag coefficients vary between 0.4 and 1.2, and the lift:drag ratios between 1.2 and 4.0. All lift coefficients are consistent with steady-state aerodynamic theory, but the highest drag coefficient seems rather high. However, Pennycuick (1971) showed that the induced drag and wing profile drag coefficients in gliding *Rousettus* rise sharply at very low speeds. At the lowest speed investigated (*ca.* 5.5 m s⁻¹) he got a summed C_D value (induced drag coeff. + wing profile drag coeff.) of *ca.* 0.32, but the extrapolated values at lower speeds were much higher. Nachtigall & Kempf (1971) measured the lift and drag coefficients of isolated wings of four bird species, and in *Passer domesticus* found a maximum lift:drag ratio of *ca.* 4.5 ($C_D = 0.25$) at an angle of attack of *ca.* 15°, and a

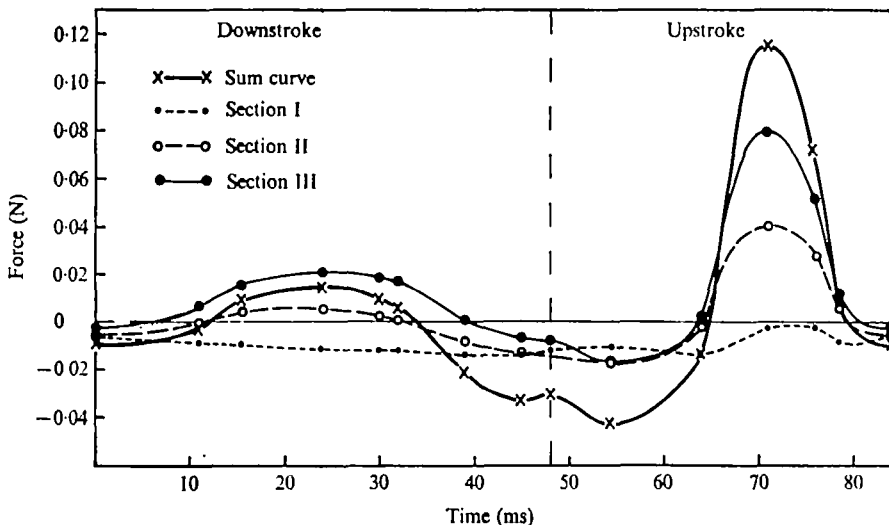


Fig. 23. Curves showing the sum of the horizontal projections of the virtual lift and drag forces, plotted against time for three sections of the wing (proximal, middle, and distal part, as indicated in Fig. 17). The summed curve for the three wing sections is also shown. Calculations based on alternative 1 (described and discussed in the text) involving a C_L value of 1.4 and a C_D value of 0.9.

ratio of ca. 1.4 ($C_D = 0.65$) at 40° . *Plecotus* uses high angles of attack in slow flight (Table 4). In view of these data the obtained highest C_D value of *Plecotus* does not seem quite so unlikely.

If L/D were larger than the largest value of *Plecotus* obtained in this investigation (4.0), the resultant force (as averaged over the wings and the whole wing-stroke) would be so inclined forward, as to make its forwardly directed horizontal component larger than the body drag. Since the flight is unaccelerated, the forward horizontal component of the resultant force must not exceed the body drag. Thus, L/D must be relatively small to keep the resultant force almost vertical and its horizontal component small enough, just matching the body drag.

The tail membrane is moving down and up during the wing-stroke, thus giving some drag but also lift in the lower half of the wing-stroke. However, this does not significantly influence the sizes of the lift and drag coefficients obtained.

RELATIVE EFFECT OF THE DOWNSTROKE AND UPSTROKE OF THE WING

The vertical and horizontal forces elicited during the wing-beat cycle are shown in Figs. 22 and 23, and are based on alternative 1, where C_L is 1.4 and C_D is 0.9 (Table 5). Fig. 24 shows the inclination of the wing chords and the direction and relative size of the lift and drag forces at three sections of the wing in three phases of the stroke cycle. It is based on case 1.

Upper reversal point. The proximal and middle sections of the wing contribute slight positive vertical forces, while the distal section gives slight negative ones. The sum of the vertical forces for the whole wing is positive. The horizontal forces elicited are negative for all wing sections.

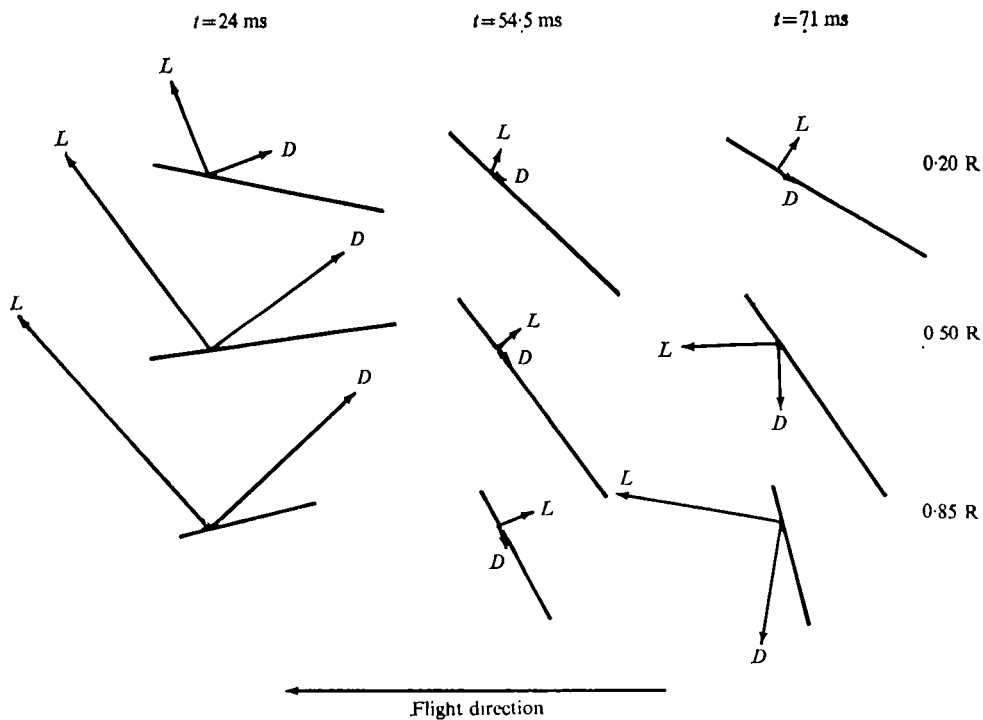


Fig. 24. The inclination of the chords of three sections of the wing (at radial distance $0.20R$, $0.50R$ and $0.85R$, respectively, from the wing hinge) and for three different phases ($t = 24$ ms: middle of the downstroke; $t = 54.5$ ms: beginning of the upstroke; $t = 71$ ms: later part of the upstroke). The directions and relative magnitudes of the forces are indicated. Based on alternative 1 (described and discussed in the text), with $L/D = 1.6$.

Downstroke. The vertical forces increase with time and reach their maximum at the middle of the downstroke ($\gamma = 110^\circ$, $t = 24$ ms). The vertical forces for the proximal part increase more slowly than for the other sections, and at $\gamma = 110^\circ$ they are only 35 % of the corresponding forces for the distal part. The sum of the vertical forces is positive during the entire downstroke.

The middle and distal sections give negative horizontal forces during the first and last part of the downstroke, and positive in the middle part. The middle section contributes positive forces during 39 % of the time of the downstroke, while corresponding measurement for the distal section is 66 %. The sum curve of the horizontal forces for the whole wing is negative the first 27 % of the duration of the downstroke, positive during the next 41 % and negative the last 32 %. However, the net value of the horizontal forces is negative.

Lower reversal point. The vertical forces are positive, and the horizontal forces are negative for all sections of the wing.

Upstroke. The base of the wing gives slight positive vertical forces during 60 % of the duration of the upstroke. For the middle and distal sections, the vertical forces are negative during 73 % of the upstroke, the parts near the reversal points being positive. The net vertical force of the whole wing is negative. Minimum is reached at $\gamma = 110^\circ$ ($t = 71$ ms).

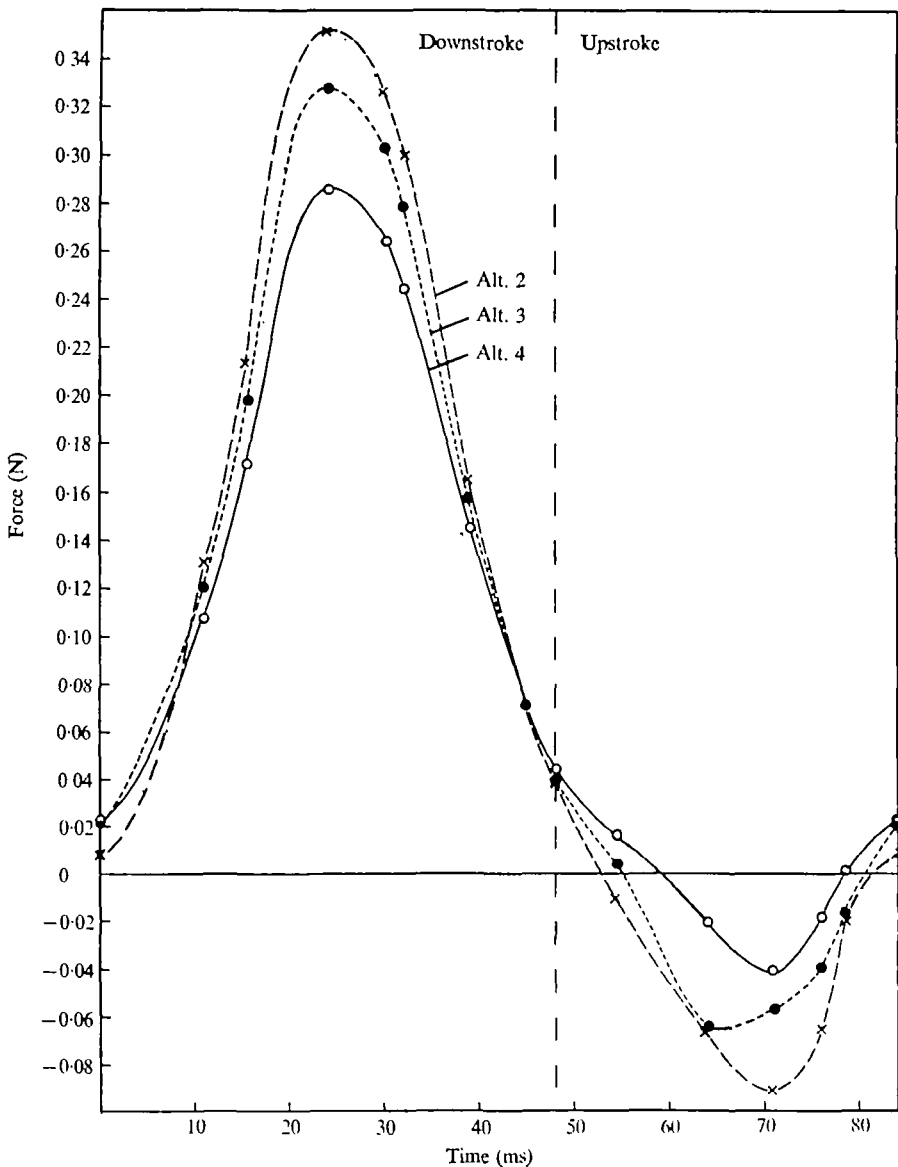


Fig. 25. Similar curves as in Fig. 22 on the vertical projections of the real lift and drag forces for the whole wing, plotted against time, but here based on three different alternatives (described and discussed in the text) with the following lift and drag coefficients: $C_L = 1.4$ and $C_D = 1.2$ (case 2), $C_L = 1.4$ and $C_D = 0.9$ (case 3), $C_L = 1.6$ and $C_D = 0.4$ (case 4).

The base of the wing contributes only negative horizontal forces during the entire upstroke. The horizontal forces elicited by the middle section of the wing are negative during the first part of the upstroke, but the force curve then increases rapidly with a peak at $\gamma = 110^\circ$. This peak is larger than that at the corresponding position during the downstroke. The horizontal force curve for the distal part of the wing follows the corresponding curve for the middle section, but crosses the zero line earlier (at $\gamma = 90^\circ$), and reaches a higher peak (at $\gamma = 110^\circ$). The sum curve of the horizontal

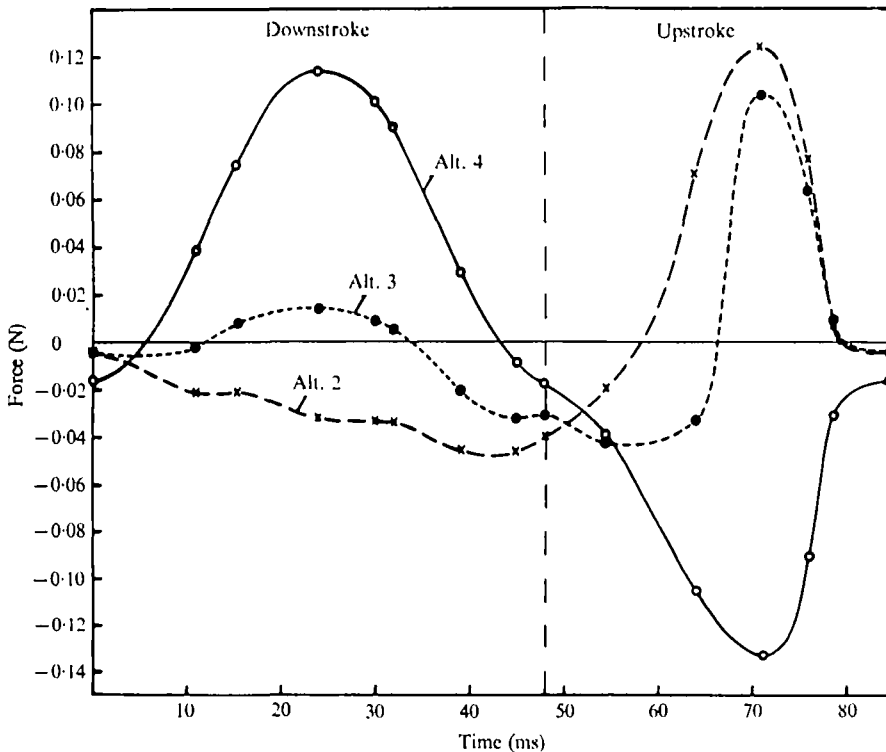


Fig. 26. Similar curves as in Fig. 23 on the horizontal projections of the real lift and drag forces for the whole wing, plotted against time, but here based on three different alternatives (described and discussed in the text) with the following lift and drag coefficients: $C_L = 1.4$ and $C_D = 1.2$ (case 2), $C_L = 1.4$ and $C_D = 0.9$ (case 3), $C_L = 1.6$ and $C_D = 0.4$ (case 4).

forces for the whole wing is negative during the first 47% of the upstroke, and also near the upper reversal point, and positive for the rest. The net value of the horizontal forces is positive.

Summarizing, the downstroke is the power stroke for the vertical forces, while in the upstroke the negative vertical forces elicited exceed the positive vertical forces (Fig. 22). Only the middle part of the downstroke and last part of the upstroke, except near the reversal point, give positive horizontal forces (Fig. 23). The upstroke contributes 86% of the total positive horizontal forces.

Figs. 25 and 26 show the vertical and horizontal force curves based on cases 2-4.

POWER REQUIREMENTS

The aerodynamic torque attributed to a wing-section is

$$Q_a(r, t) = rM(r, t), \quad (31)$$

where $M(r, t)$ is the component in the stroke plane of the resultant force.

$$M(r, t) = r^2 \rho V_R^2(r, t) A(r) C_L \sin(\chi + \psi + \beta) / \cos \chi, \quad (32)$$

as can be seen in Fig. 19. The extremes of the calculated average lift:drag ratios and

drag coefficients (Table 5, alternatives 2 and 4) were used to get the maximum and minimum values of the aerodynamic work and power.

The inertial torque (i.e. the bending moment caused by the acceleration of the wing-mass in the stroke plane) is

$$Q_i = I\ddot{\gamma}(t) = -2I\phi\pi^2n^2 \sin(2\pi nt) \quad (33)$$

(cf. equation (1)), where I is the moment of inertia of the wing-mass with respect to the fulcrum. I equals $m(r) r^2$, where $m(r)$ is the mass of a chordwise wing strip at distance r from the fulcrum. Data from Table 3 was used.

The total work produced by the wing-stroke muscles during one wing-stroke is the sum of the work done during the downstroke and during the upstroke, and is

$$W_t = \int_{\gamma_{\max}}^{\gamma_{\min}} (Q_a + Q_i) dy + \int_{\gamma_{\min}}^{\gamma_{\max}} (Q_a + Q_i) dy. \quad (34)$$

The total mechanical power imparted by the wing muscles to the wings is then

$$P = nW_t = n \left[\int_{\gamma_{\max}}^{\gamma_{\min}} (Q_a + Q_i) dy + \int_{\gamma_{\min}}^{\gamma_{\max}} (Q_a + Q_i) dy \right]. \quad (35)$$

To make the results directly comparable with other authors' measurements on other animals (e.g. Weis-Fogh, 1972, 1973; Thomas, 1975) the torque, work, and power are divided by the total mass of the animal in question, thus giving *specific* torque, work, and power, respectively. An asterisk after the symbol indicates that the quantity is specific as defined above.

Aerodynamic torque and work. The aerodynamic torque was calculated for the three sections into which the wing was divided and for 14 positions distributed over the wing-stroke as indicated in radians (positional angle) in Fig. 27. The specific aerodynamic torque, Q_a^* (i.e. the aerodynamic bending moment per unit body mass), is illustrated in the work diagram in Fig. 27 (the vertical distance between curve and abscissa). The area enclosed by the curve $ABEFGA$ is the positive aerodynamic work done during one complete wing-stroke. The area $EFGAE$ represents the positive work done during the downstroke (γ_{\max} to γ_{\min}), and the area ABA represents the positive work done during the upstroke (γ_{\min} to γ_{\max}).

Four different alternative assumptions were made regarding the orientation of the zero-lift line. In case 4, the aerodynamic angles of attack (relative to the zero-lift line) were assumed to be positive in all phases and over the whole wing during the entire upstroke. The consequence of this is that the vertical force component as averaged over the whole wing is directed upwards in some sections and phases of the upstroke. Furthermore, the aerodynamic force as projected on the stroke plane is then directed in the same direction that the wing is moving. The acceleration of the wing (in the beginning of the upstroke) is then influenced positively by the air (i.e. the wing gains aerodynamic work from the air), this being termed negative aerodynamic work (with corresponding negative torque). In the decelerating phase of the upstroke the negative aerodynamic work is matched by negative work of the muscles and disregarded here for the reason discussed below.

In case 2, airflow angles $\leq -10^\circ$ are assumed to be negative angles of attack. This gives negative aerodynamic work in the beginning and end of the upstroke (Fig. 27).

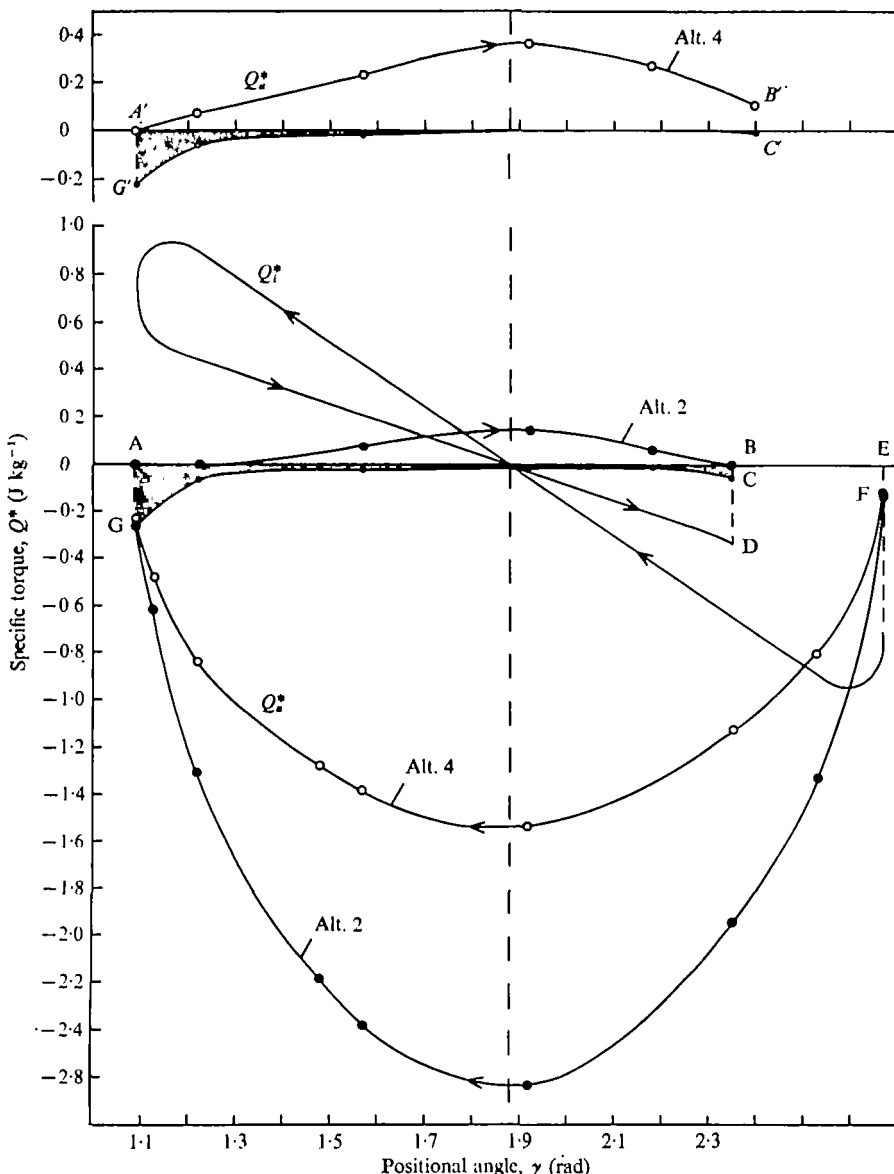


Fig. 27. Work diagram of the bat in horizontal flapping flight at a flight speed of 2.35 m s^{-1} and a flapping frequency of 11.9 Hz . The curves show the specific aerodynamic torque, Q_a^* , and the specific inertial torque, Q_t^* , in two cases (namely, case 2 with $C_L = 1.4$ and $C_D = 1.2$, and case 4 with $C_L = 1.6$ and $C_D = 0.4$, described further in the text) during a complete wing-stroke. The downstroke is represented by the curve FG and the upstroke by AB ($A'B'$) and GC ($G'C'$). The torque is of positive sign when it tends to turn the wing in the morphologically downward direction. The shaded areas show specific aerodynamic work of negative sign during the upstroke. The stroke angle of the upstroke is somewhat less than during the downstroke in this particular wing-stroke. This difference is of little significance for the result.

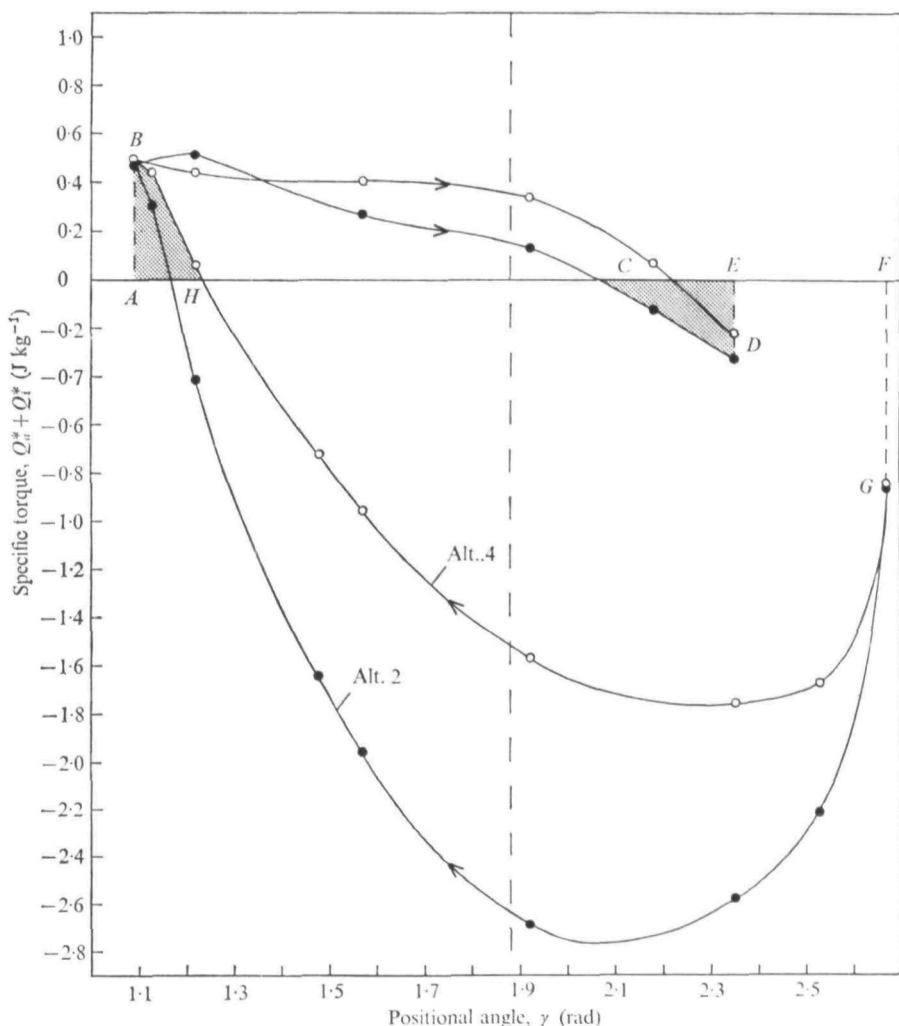


Fig. 28. The summed specific torque, $Q_a^* + Q_i^*$, obtained from Fig. 27. The areas $FGHF$ and $BCHB$ represent the total positive work that must be done by the wing-stroke muscles during the downstroke and upstroke, respectively. The shaded areas indicate negative muscular work during the downstroke ($ABHA$) and upstroke ($CEDC$), respectively, provided that there is no energy-saving elastic system (elastic counter-torque).

Inertial torque and work. To estimate the inertial torque, the wing was divided into 12 strips, and the mass measured, and moment of inertia calculated for each strip (Fig. 17). During the upstroke the radii are reduced by wing flexion (see p. 195), thus strongly reducing the moment of inertia. The specific inertial torque Q_i^* changes sign during the wing-stroke. Positive sign of the specific inertial torque indicates that the force is directed in the morphological dorsal direction, and negative sign that the force is directed in the morphological ventral direction.

Total work. The torque which the wing-stroke muscles have to produce is obtained by adding Q_a^* and Q_i^* for every wing position separately, as in Fig. 28. The negative aerodynamic torque helps to accelerate the wing during the first half of the upstroke

from 1.09 rad to 1.88 rad). Therefore, this aerodynamic torque relieves the wing elevating muscles of some of their torque and hence should be subtracted from the inertial torque. Area *ABCA* represents the positive work which the muscles must deliver to the wings during the first part of the upstroke. During the last part of the upstroke, the downstroke muscles have to brake the movement and absorb the excess kinetic energy of the wings. The angular momentum of the wings thus causes a stretching of the downstroke muscles which actively resist stretching. Work done during stretching of a muscle is termed negative work and here has a magnitude indicated by the area *CDEC*. During the downstroke the positive work in Fig. 28 is represented by the area *FGHF*, while the area *ABHA* is negative work. As performed by striated muscles, negative work costs only about 20% in metabolic energy (in human locomotion; Margaria, 1968) of the same amount of positive work. In the bat the negative work then would add less than 1% to the total amount of positive work. Following Weis-Fogh (1972, p. 91), the negative work is disregarded here, in order not to exaggerate the estimate of work and power.

Areas *ABCA* and *FGHF* together represent the minimum amount of work per wing-stroke.

The specific positive aerodynamic work in Fig. 27 is $W_a^* = 3.33 \text{ J kg}^{-1}$ when $C_L = 1.4$ and $C_D = 1.2$ (alternative 2 in Table 5). The corresponding specific work when $C_L = 1.6$ and $C_D = 0.4$ (alternative 4) is $W_a^* = 2.91 \text{ J kg}^{-1}$. Henceforth the results with alternative 4 are set within parentheses. The aerodynamic work done during the upstroke is only 2.6% (12.8%) of the aerodynamic work done during one complete wing-stroke. This is due to the flexing of the wings during the upstroke, which decreases the flapping speed of the wings and the wing area, and also to the fact that some aerodynamic work is negative, i.e. not supplied actively by the muscles.

The specific inertial work W_i^* is also less during the upstroke than during the downstroke depending on the reduced radii of the wing strips. In Fig. 27 $W_i^* = 0.62 \text{ J kg}^{-1}$, of which ca. 34% is done during the upstroke. The inertial work is thus reduced with ca. 48% during the upstroke as a result of the wing flexion. The direct sum of the specific positive aerodynamic and inertial work ($W_a^* + W_i^*$) is 3.95 J kg^{-1} (2.83 J kg^{-1}). During a complete wing-stroke the sum of the specific aerodynamic and inertial positive work in Fig. 28 is 3.40 J kg^{-1} (2.27 J kg^{-1}). About 0.07 J kg^{-1} (0.06 J kg^{-1}), or ca. 2.0% (2.6%), of the total mechanical work is wasted. This wasted work is inertial work (areas *ABHA* and *CEDC* in Fig. 28) which has not been converted into aerodynamic work.

Total power. With a stroke frequency of 11.9 Hz the total specific mechanical power output of the wing muscles is $P^* = 11.5 \times 3.40 = 40.5 \text{ W kg}^{-1}$ ($11.5 \times 2.27 = 27.0 \text{ W kg}^{-1}$). The total power output during the upstroke is only 8% (18%) of that during the complete wing-stroke. These values of total mechanical power output are arrived at via mechanical and aerodynamical calculations. One way of judging the plausibility of the values and, thus, of the concept of steady-state aerodynamics in bat flight, is to compare them with the actual power output of flying bats. If the calculated total mechanical power is not more than 20–30% of the metabolic rate it can be regarded as plausible.

Data is not available on the metabolic rate of *Plecotus* in flight (or at rest). Therefore,

these have to be estimated with the aid of known data of other bats in flight. Thomas & Suthers (1972) measured the oxygen consumption of *Phyllostomus hastatus* in flight. In seven specimens, weighing 0.853 N and flying about 4.5 min at 3.6 m s⁻¹, the average specific metabolic rate was 24.7 ml O₂ (gh)⁻¹ = 143.5 W kg⁻¹ (1 ml O₂ = 5 cal = 20.92 J if fat is the fuel). In a later investigation Thomas (1975) measured the metabolism during flight again in *Phyllostomus hastatus* and in *Pteropus gouldii*. Maximum mean metabolic rate of *Phyllostomus hastatus* (mean body weight 0.912 N) was 130.4 W kg⁻¹ and in *Pteropus gouldii* (mean body weight 7.65 N) it was 69.6 W kg⁻¹.

The power required to fly at a special speed (such as minimum power speed or maximum range speed) is proportional to the $\frac{7}{6}$ power of the body mass for geometrically similar animals (Pennycuick, 1969). On the other hand the basal metabolism would scale about $\frac{4}{3}$ power of the body mass (Lasiewski & Dawson, 1967). *Plecotus* and the bats in Thomas' investigation were not flying at corresponding speeds and are not geometrically similar. Therefore, it is extremely difficult to make a comparison between the bats regarding the metabolic rate during flight. However, presently available data from bats (Thomas, 1975) and birds (Tucker, 1973) in level flight fall along a straight line when the minimum metabolic rate per unit body mass (i.e. power input per unit body mass at the speed where cost of transport is minimum), $P'_{t,0}$, is plotted on double logarithmic coordinates against body mass. The least-squares equation fitted to these data is given by Thomas (1975), and is

$$P'_{t,0} = 58.4m_b^{-0.81}, \quad (36)$$

where m_b is body mass.

Using equation (36) for *Plecotus*, its minimum metabolic rate becomes 157 W kg⁻¹. The true minimum value may be somewhat larger because of the bat's big ears. Using 157 W kg⁻¹ as a minimum value, the *maximum mechanical efficiency* during slow forward flight in *Plecotus* would be $40.5/157 = 0.26$ ($27.0/157 = 0.17$). Both values are very reasonable. Tucker (1972), for example, empirically found the mechanical efficiency for laughing gull (*Larus atricilla*) to be between 0.19 and 0.28 at various flight speeds. He used respiration data from a gull flying actively in a wind tunnel that was tilted to various degrees, thus forcing the bird to perform descending or ascending flight of various steepness. With the same method the mechanical efficiencies were found to be 0.20–0.26 for a fish crow (*Corvus ossifragus*; Bernstein, Thomas & Schmidt-Nielsen, 1973), 0.12–0.40 for *Phyllostomus hastatus*, and 0.22–0.31 for *Pteropus gouldii* (Thomas, 1975).

The true mechanical efficiency for *Plecotus* in slow horizontal flight is difficult to estimate, since the bat was flying below its minimum power speed (see below), and, therefore, needed a much higher metabolic rate than 157 W kg⁻¹. However, 0.26 can be regarded as a maximum value of the efficiency. Since this is a reasonable value of the mechanical efficiency this knowledge is enough to warrant the conclusion that steady-state aerodynamics may very well prevail (as far as this test goes).

Aerodynamic efficiency. The induced velocity at the level of the disc is $V_t = 0.27$ m s⁻¹. The induced power then becomes $P_{ind} = WV_t \leq 0.0238$ W, and the specific induced power $P_{ind}^* = 2.65$ W kg⁻¹. The specific aerodynamic power is $P_a^* = 3.33 \times 11.9 = 39.6$ W kg⁻¹ ($2.21 \times 11.9 = 26.3$ W kg⁻¹). As compared with an ideal actuator

lisc the aerodynamic efficiency then is $2.65/39.6 = 0.07$ ($2.65/26.3 = 0.10$). These values are rather low. However, because of the high drag coefficients, one should expect a low aerodynamic efficiency. This is because L/D must be relatively small to keep the resultant force almost vertical, and its horizontal, forward, component small enough. This also gives a large component of the resultant force in the stroke plane, M_r . Therefore, the obtained values on the aerodynamic efficiency are explainable and very plausible.

MINIMUM POWER SPEED

The minimum power speed, V_{mp} , is the speed at which the power required to fly is at minimum. Pennycuick (1969) devised the following formula for computation of V_{mp} :

$$V_{mp} = \frac{0.76 W^{\frac{1}{4}}}{\rho^{\frac{1}{4}} A_e^{\frac{1}{4}} S_d^{\frac{1}{4}}}. \quad (37)$$

The large ears in *Plecotus* have a frontal area of ca. 65 % of that of the body. V_{mp} for *Plecotus* then becomes 3.1 m s^{-1} . Hence, the speed of the flight analysed in this paper is somewhat lower than the minimum power speed. By flying a bit faster, the bat will probably reduce the power output.

CONCLUSION

One of the problems was to discover if slow horizontal flight in *Plecotus* is consistent with steady-state aerodynamics, or if it has to be explained partly, or mainly, by non-steady state phenomena. The hypothesis of steady-state aerodynamics was tested in two ways:

(1) by finding out if the average coefficients of lift and drag, C_L and C_D , arrived at via calculations based on steady-state aerodynamics, are consistent with the wing-profile and Reynolds number in question, and

(2) by finding out if the mechanical efficiency is plausible. The mechanical efficiency is obtained by relating data on specific power output, arrived at via mechanic and steady-state aerodynamic calculations, to data on actual specific metabolic rate of bats in flight.

The conclusions are as follows. The Reynolds number (Fig. 16) is ca. 18500 at $0.7R$ in the middle of the downstroke. The lift coefficients obtained then are consistent with steady-state aerodynamics. Since the bat may be expected to use high angles of attack at this slow flight speed (and was also found to do so from the films) to attain high lift coefficients, the drag coefficients are expected to be high. However, the value 1.2 is very high for a drag coefficient and the question is whether it is likely to occur in the bat. To find this out one may go further and see if the mechanical efficiency at this value is plausible.

The two extreme value sets of C_L and C_D (case 2 and 4 respectively, p. 197) were used in the calculations of work and power to get the extreme values of these quantities that would follow if steady-state aerodynamics prevail.

The force coefficients, total mechanical power output, and mechanical efficiency (associated with alternatives 2 and 4) are plausible, thus demonstrating that steady-

state aerodynamics may very well prevail. However, it is not excluded that non-steady-state periods are involved. Alternatives 1 and 3 give values between the extremes and are then also explainable by steady-state aerodynamics.

Since the bat uses non-steady-state aerodynamics to a considerable degree in hovering flight (Norberg, in preparation), these non-steady-state mechanisms (whatever they are) may very well be utilized to some degree also in slow horizontal flight. It is also conceivable that steady-state and non-steady-state mechanisms act together. Nevertheless, the main conclusion remains, namely that steady-state aerodynamics are sufficient to explain slow horizontal flight. If non-steady-state aerodynamics are involved, the steady-state aerodynamics are likely to be the most important part of the explanation of the flight.

DISCUSSION

The wing-stroke path relative to the body was not quite closed in the wing-stroke chosen for analysis (i.e. the stroke angle of the upstroke, 72.2° , was less than during the downstroke, 90.7°). This has been taken into account in the different calculations.

The drag coefficients obtained are high, but at low speeds one can expect a high value of C_D and a low lift/drag ratio. This is so because an animal flying at low speeds must work with high angles of attack to obtain sufficient lift, which necessarily brings with it high drag coefficients. The minimum power speed for *Plecotus* is calculated to be about 3.1 m s^{-1} . This is a little faster than the flight speed analysed. The question thus arises as to whether the bat normally cruises about at these low speeds. Its main feeding habitat is broad leaf tree crowns, where it hunts insects among the branches and even *on* the leaves. It is very adept at manoeuvring in narrow spaces and often hovers, for instance when picking insects from branches and leaves. My experience from field observations is that *Plecotus* often flies very slowly, especially in dense vegetation (tree crowns).

The remarkably large ears must catch the echoes from the emitted echolocation signals very effectively, and improve the ability to discover small objects, for example insects, on leaves. One might suggest that only a bat which specializes in low-speed flight can afford to have big, drag-producing, ears. At low speeds the bat's main expense is induced power and the addition of more frontal area, and hence parasite power, does not make much difference to the total power. In fact, it is only low-speed, low aspect ratio bats, which have large, projecting ears. Except for *Plecotus*, for example, the genera *Lavia*, *Nycteris*, *Euderma*, *Macrotus* all possess big erect ears. My films on flying specimens of *Lavia* and *Nycteris* show that their flight is very slow and manoeuvrable. As a rule, broad wings (low aspect ratio wings) are associated with slow flight.

The low-speed, horizontal flight in *Plecotus* can be explained by steady-state aerodynamics. However, one cannot exclude the possibility that non-steady state phenomena may be involved in some periods of the stroke. In some insects a rapid twist of the wings at the reversal points builds up lift generating circulation around the wings (the 'flip' mechanism, Weis-Fogh, 1973). In *Plecotus* there is a pitching rotation at the top and bottom of the stroke (Fig. 14) about a spanwise axis, located *ca.* 40% of the chord length behind the leading edge (at the level of the fifth digit), which might give some lift generating circulation around the wings. Although it is doubtful whether

his rotation is rapid enough, the possibility remains that it may be of some importance.

In the calculations no energy-saving elastic system has been taken into account. Yet, only *ca.* 2·0–2·6 % of the total mechanical work is wasted in *Plecotus*. Therefore, an energy-storing elastic system would not be of any great importance in horizontal flight in *Plecotus*.

The bat wing membrane is a highly elastic structure which contains the protein elastin. Furthermore, in *Plecotus*, as in many other bat species, the tips of the third, fourth, and fifth digits are cartilaginous and flexible (Norberg, 1970b). These structures might be of some importance for absorption and release of elastic energy at the top and bottom of the stroke. However, the elastic properties of these structures are not known, so it remains uncertain to what extent they could release any energy absorbed.

Schaefer (1975) suggested that the clavicle may be used for storage and release of kinetic energy in birds.

Insects have a highly elastic, energy-saving, wing-system of which the major contribution derives from the sclerotized cuticle of the thorax and from the rubber-like ligaments whose main component is the protein resilin (Weis-Fogh, 1965). Since the inertial power is relatively high in insects (because of the high wing beat frequencies), the elastic wing-system is of considerable importance for energy saving in insect flight. Indeed, many insects would not be able to produce the power necessary to fly if they lacked the elastic energy-storing wing-system.

I am greatly indebted to Dr C. J. Pennycuick, Dept. of Zoology, University of Bristol, for reading and commenting upon the manuscript, and to Prof. Sir J. Light-hill for discussion on part of the manuscript. I also thank Prof. T. Eeg-Olofsson, Chalmers Univ. of Technology, Göteborg, for making available a high-speed film camera, and Civ.-ing. K. Pehrsson and Ing. R. Nilsson, Chalmers Univ. of Technology, for filming aid. Further I thank Miss B. Karlson and Miss Eva Myrin for typing aid and Mrs Aino Wahlström for drawing some of the figures.

REFERENCES

- ABBOTT, I. H. & VON DOENHOFF, A. E. (1959). *Theory of Wing Sections*, 2nd ed. New York: Dover.
- BERNSTEIN, M. H., THOMAS, S. P. & SCHMIDT-NIELSEN, K. (1973). Power input during flight of the fish crow, *Corvus ossifragus*. *J. exp. Biol.* **58**, 401–10.
- BETZ, E. (1958). Untersuchungen über die Korrelation der Flugmechanismen bei den Chiropteren. *Zool. Jahrb. (Abt. Anat.)* **77**, 491–526.
- LASIEWSKI, R. C. & DAWSON, W. R. (1967). A re-examination of the relation between standard metabolic rate and body weight in birds. *Condor* **69**, 13–23.
- MARGARIA, R. (1968). Positive and negative work performances and their efficiencies in human locomotion. *Int. Z. angew. Physiol. einschl. Arbeitsphysiol.* **25**, 339–51.
- NACHTIGALL, W. & KEMPF, B. (1971). Vergleichende Untersuchungen zur flugbiologischen Funktion des Daumenfittichs (*Alula spuria*) bei Vögeln. I. Der Daumenfittich als Hochauftriebserzeuger. *Z. vergl. Physiol.* **71**, 326–41.
- NORBERG, R. Å. (1975). Hovering flight in the dragonfly *Aeschna juncea*. In: Wu, T. Y.-T., Brokaw, C. J. and Brennen, C. (eds.): *Swimming and Flying in Nature*, vol. 2, pp. 763–81. New York: Plenum Publ. Corp.
- NORBERG, U. M. (1969). An arrangement giving a stiff leading edge to the hand wing in bats. *J. Mamm.* **50**, 766–70.
- NORBERG, U. M. (1970a). Hovering flight of *Plecotus auritus* Linnaeus (Chiroptera). *Bijdr. Dierk.* **40** (Proc. 2nd Int. Bat Res. Conf.), 62–6.

- NORBERG, U. M. (1970b). Functional osteology and myology of the wing of *Plecotus auritus* Linnaeus (Chiroptera). *Ark. Zool.* **22** (12), 483–543.
- NORBERG, U. M. (1975). Hovering flight in the pied flycatcher *Ficedula hypoleuca*. In: Wu, T. Y.-T., Brokaw, C. J. and Boennen, C. (eds.): *Swimming and Flying in Nature*, vol. 2, 869–81. New York: Plenum Publ. Corp.
- NORBERG, U. M. (1976). Aerodynamics of hovering flight in the long-eared bat *Plecotus auritus*. *J. exp. Biol.* (in the Press).
- PANKHURST, R. C. (1944). A method for the rapid evaluation of Glauert's expressions for the angle of zero lift and the moment at zero lift. Aeronautical Council R & M no. 1914.
- PENNYCUICK, C. J. (1968). Power requirements for horizontal flight in the pigeon *Columba livia*. *J. exp. Biol.* **49**, 527–55.
- PENNYCUICK, C. J. (1969). The mechanics of bird migration. *Ibis* **111**, 525–56.
- PENNYCUICK, C. J. (1971). Gliding flight of the dog-faced bat *Rousettus aegyptiacus* observed in a wind tunnel. *J. exp. Biol.* **55**, 833–45.
- PENNYCUICK, C. J. (1972). *Animal Flight*. Studies in Biology, no. 33. London: Edward Arnold.
- PENNYCUICK, C. J. (1973). Wing profile shape in a fruit-bat gliding in a wind-tunnel determined by photogrammetry. *Period. biol.* **75**, 77–82.
- SCHAEFER, G. W. (1976). Dimensional analysis of avian forward flight. Paper read at the *Symp. on Biodynamics of Animal Locomotion*, Cambridge, 1975 (in the Press).
- SCHNITZLER, H.-U. (1971). Fledermäuse im Windkanal. *Z. vergl. Physiol.* **73**, 209–21.
- THOMAS, S. P. & SUTHERS, R. A. (1972). The physiology and energetics of bat flight. *J. exp. Biol.* **57**, 317–35.
- THOMAS, S. P. (1975). Metabolism during flight in two species of bats, *Phyllostomus hastatus* and *Pteropus gouldii*. *J. exp. Biol.* **63**, 273–93.
- TUCKER, V. A. (1972). Metabolism during flight in the laughing gull (*Larus atricilla*). *Am. J. Physiol.* **222**, 237–45.
- TUCKER, V. A. (1973). Bird metabolism during flight: evaluation of a theory. *J. exp. Biol.* **58**, 689–709.
- WEIS-FOGH, T. (1965). Elasticity and wing movements in insects. *Proc. XIIth Int. Congr. Ent.* pp. 186–8.
- WEIS-FOGH, T. (1972). Energetics of hovering flight in hummingbirds and in *Drosophila*. *J. exp. Biol.* **56**, 79–104.
- WEIS-FOGH, T. (1973). Quick estimates of flight fitness in hovering animals, including novel mechanisms for lift production. *J. exp. Biol.* **59**, 169–230.